Improved Kyoto University Cyclotron (Memorial Issue Dedicated to the Late Professor Yoshiaki Uemura)

AUTHOR(S):

Uemura, Yoshiaki; Fukunaga, Kiyoji; Kakigi, Shigeru; Yanabu, Takuji; Fujiwara, Noboru; Ohsawa, Takao; Fujita, Hirokazu; Miyanaga, Toshihiro; Nguyen, Dai Ca

CITATION:

Uemura, Yoshiaki ...[et al]. Improved Kyoto University Cyclotron (Memorial Issue Dedicated to the Late Professor Yoshiaki Uemura). Bulletin of the Institute for Chemical Research, Kyoto University 1974, 52(1): 87-123

ISSUE DATE:

1974-07-25

URL:

http://hdl.handle.net/2433/76537

Bull. Inst. Chem. Res., Kyoto Univ., Vol. 52, No. 1

Improved Kyoto University Cyclotron

Yoshiaki UEMURA*, Kiyoji FUKUNAGA, Shigeru KAKIGI**,
Takuji YANABU, Noboru FUJIWARA, Takao OHSAWA,
Hirokazu FUJITA, Toshihiro MIYANAGA, and Dai Ca NGUYEN***

Received January 8, 1974

The 105 cm Kyoto University Cyclotron built in 1952 through 1955 had expired its life span and have been remodeled since 1969. All parts of the old cyclotron were replaced with new ones except the main magnet. Efforts were paid to increase the beam intensity, to make the beam energy variable, to accelerate various kinds of ions and to get simple handling and reliable control. The design principle and the performance characteristics of ion acceleration with the renewed cyclotron are described.

I. INTRODUCTION

The Kyoto University Cyclotron was built in 1952 through 1955 and the characteristics of this cyclotron are reported in Ref.[1] This cyclotron has been utilized to promote researches in the field of nuclear science, and papers more than 70 have been published[2] in which the results obtained by using this cyclotron are described. However, after ten years hard operation, troubles began to occur frequently since 1965. Small motors to drive the frequency compensator, rectifiers of the high voltage source of the deflector and so on went wrong one after another. There happened also some peculiar diseases such as the burning up of polystylene insulators used in a R. F. feeder line. By and by, water cooling pipes inside the acceleration vacuum chamber began to leak. Repairing and test operation of the cyclotron took almost of the time and the yearly beam time for the experiments decreased rapidly. Because there have been few reports on the deterioration of cyclotrons, and we in Japan have no experience of long term cyclotron operation, it was not clear for us at that stage that how and what part of the cyclotron began to be damaged. However, when the history of damage affairs in our laboratory were compiled, it became clear that the characteristics of damage affairs changed from complicated ones to simple, mechanical affairs. The things were getting worse. In the fall of 1967, it was concluded that the life span of the cyclotron expired and a plan to renew the cyclotron should be established as quickly as possible. In fact, at the end of 1969, the beam extraction became impossible because of the failure of the deflector and the feasibility of the cyclotron had ceased. Since then, this cyclotron was used as merely a test load of the new R. F. oscillator to clarify the multipactoring

* 故植村吉明: The late lamented. Nuclear Science Research Facility, Institute for Chemical Research, Kyoto University.

** 福永清二, 柿木 茂: Nuclear Science Research Facility, Institute for Chemical Research, Kyoto University, Kyoto

*** 柳父琢治, 藤原 昇, 大澤孝夫, 富士田浩一, 宮永俊博, 阮 大哥: Laboratory of Nuclear Reaction, Institute for Chemical Research, Kyoto University, Kyoto.

phenomenon. The cyclotron was shut down since March of 1970. After one year's time interval to cool down the residual radioactivities inside the acceleration chamber, the chamber, the co-axial resonant lines, dees, and other equipments were decomposed and removed. The residual radioactivities were studied after the decomposition and the results are reported in other paper in this Bulletin.

At the beginning of the design study, it was thought to convert the cyclotron from this ordinary type to an azimuthaly varying field type, but the cost and man power estimation forced us to abandon this conversion plan. Another important condition was that the remodeling of the cyclotron should be completed as short as possible so as not to suffer from long term interruption of researches. Two years of construction was scheduled and the design study was carried out under the condition that the magnetic field of the renewed cyclotron is provided by the present magnet and pole tips. Hereafter, we call the cyclotron before and after the remodeling the old one and the new one respectively.

The old cyclotron was designed to get as high energy and intense beam as possible by the use of a 105 cm magnet. Therefore, the magnetic field was adjusted to give best field distribution at 17.5 kG.. The Rose shim of the pole tip had dimensions of twice as large as theoretical values taking into account the magnetic saturation of the pole tip materials. This large Rose shim caused a radially increasing field near the position of the deflector at magnetic field strength below 12 kG and cause defocusing of the beam. Available lower limit of the magnetic field was estimated to be 15 kG. or so, and the range of energies and of kinds of particles to be accelerated were selected as in Fig. 1–1. Design principles were decided, after several times of discussions among authors of this report, as follows.

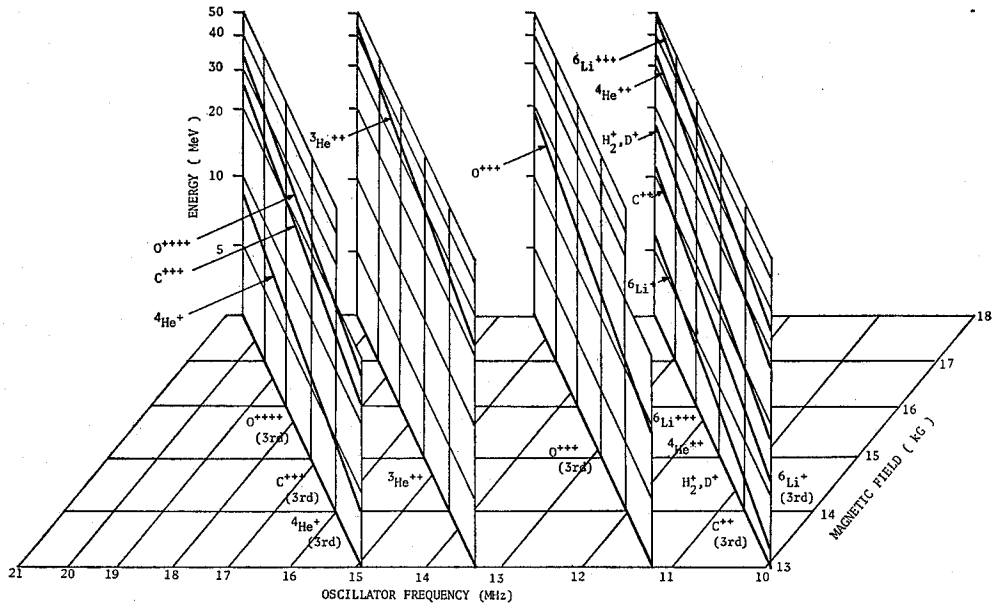

Fig. 1–1. A three dimensional representation of the range of magnetic field, frequency and energy of accelerated ions with the improved cyclotron.

1. The new cyclotron should be able to accelerate ^{3}He and heavy ions besides the ions accelerated with the old cyclotron.

2. The new cyclotron should produce beams of various energy of which the range should be as wide as possible.

3. The new cyclotron should produce more than five times as intense beam of 0.1% energy spread as that of the old cyclotron.

4. The new cyclotron should be much more stable and easier to handle than the old cyclotron.

Comparison is made in Table I about what differences exist between the old and new cyclotron. In the following sections, details of the design parameters and performance characteristics of the renewed cyclotron are described. This paper deals with the present status of the cyclotron. Acceleration of ^{3}He ions and of other kind ions at various energies will be reported separately in near future.

Table I. Differences between the Old and New Cyclotron.

Items	Before remodeling (old cyclotron)	After remodeling (new cyclotron)
Main magnet	pole tip 105 cm	no difference
Magnetic field	17.5 kG	15 kG–17.5 kG
Gap between pole tips	135 mm	144 mm
Type of dee	double dees	single dee
Dee voltage	dee to dee 100 kV	dee to ground 100 kV
Position of deflector	inside the dee	outside the dee
Deflector voltage	45 kV	100 kV
Magnetic channel	none	3 rods system
Resonant cavity	double quarter wave lines	single quarter wave line
Dimensions of cavity	inner shell 200 mm	inner shell 400 mm
	outer shell 600 mm	outer shell 1,200 mm
Line termination	shorting condenser	shorting plate
Resonant frequency	13 MHz	11–18 MHz
Type of oscillator	D. C. biased oscillator	booster and main oscillator
Osc. power tube	8T71 × 2	7T40 + 9T82
Oscillator out put	75 kW	120 kW
Coupling of osc. to resonant cavity	L-coupling	C-coupling
Main evacuating pump	2,500 *l*/s o.d.p. × 2	10,000 *l*/s o.d.p. × 1. Oil 4.2 *l*
Booster pump	80 *l*/s o.d.p.	800 *l*/s o.d.p.
Helium leak detector	none	equipped to the main pump
Type of ion source	single arm, hooded arc	dual arm, hooded arc
I. S. arc voltage	300 V single stage	300 V + 500 V, two stage
Lithium ion source	none	metal bombarded by electrons
Beam energies	H 7.5 MeV	6–7.5 MeV
	D 15 MeV	12–15 MeV
	He (3)	30–40 MeV
	He (4) 30 MeV	24–30 MeV
	Li (6)	max. 44 MeV

II. MAGNET AND MAGNETIC FIELD

The magnet of the renewed cyclotron is the same as that of the old cyclotron. Pole tips used in the old cyclotron are still used in the new cyclotron, but the method of pole tip supporting and the shimming gap length were altered. In the new cyclotron, each pole tip is fixed to a ring shaped frame made from non magnetic stainless steel (SUS32) and three pillars located symmetrically join the both frames together to maintain a fixed separation length and the centering of both pole tips. Pillars are also made from SUS 32. Pole tips and the supporting system are inserted as a whole into the gap between the magnet poles. Shimming gap of 1.6 mm remains between the pole and the pole tip. The gap length is kept constant even when the magnet is excited by placing a central aluminum spacer of 100 mm in diameter and nine pieces of aluminum plate of 20×10 mm^2 around the periphery. Figure 2–1 shows the cross sectional view of the pole, pole tip, and other components.

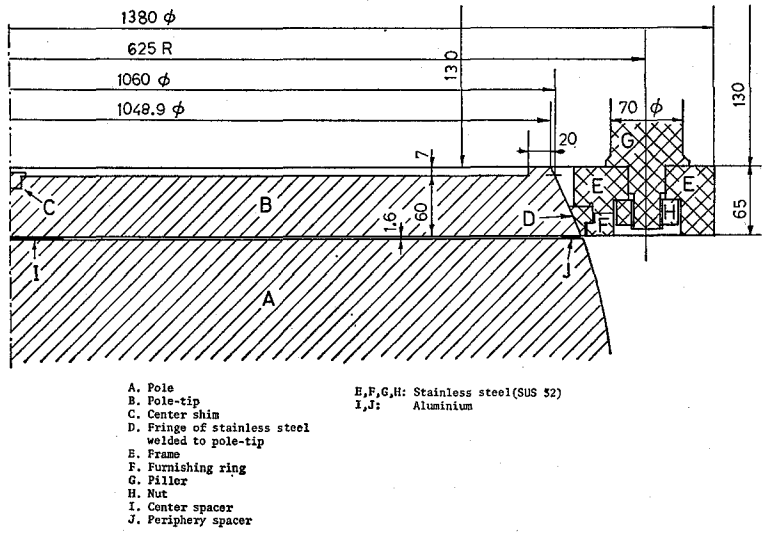

A. Pole
B. Pole-tip
C. Center shim
D. Fringe of stainless steel welded to pole-tip
E. Frame
F. Furnishing ring
G. Piller
H. Nut
I. Center spacer
J. Periphery spacer

E,F,G,H: Stainless steel(SUS 32)
I,J: Aluminium

Fig. 2–1. Cross sectional view of the pole, the pole tip and the pole tip supporting frame.

The distribution of the gap length between two pole tip faces was measured with a screw micrometer made from non-magnetic brass when the magnet was excited. In a case where the exciting current was 130 A, the azimuthal distribution of the gap length has a scatter of 0.02 mm at a radius of 105 mm and a scatter of 0.08 mm at a radius of 455 mm. The radial distribution of the gap length is monotonously decreasing. The magnitude of radial decrease is less than 0.13 mm in the range from 105 mm radius to 455 mm radius.

The magnetic field distribution was measured along the median plane with a differential type gauss meter with two Hall probes. This gaussmeter is not calibrated and so the indication contains some errors. Figure 2–2 shows the radial distributions of the magnetic field in cases of $I = 120$ A and 70 A. The ordinate gives the deviation of the

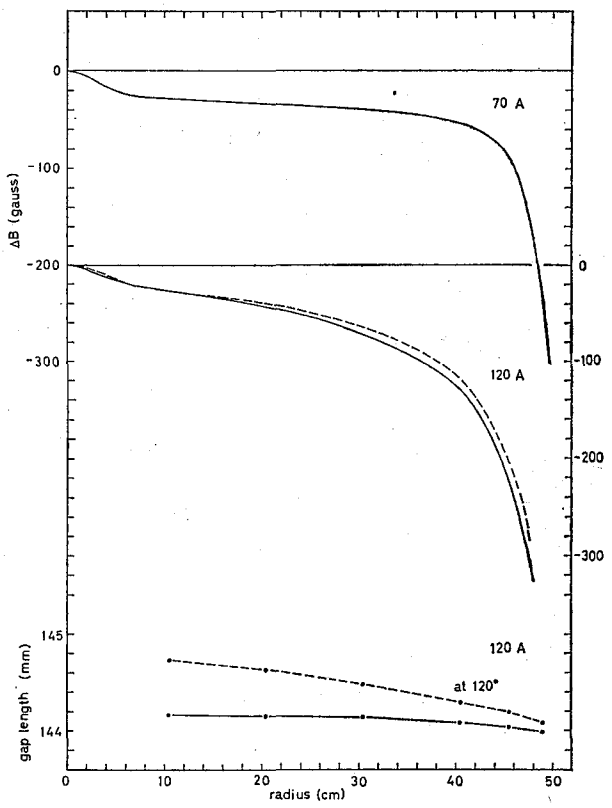

Fig. 2–2. Radial distribution of the magnetic field. Exciting current is 120 A and 70 A respectively.

magnetic field from the standard one. The solid line in the figure shows the radial distribution of the magnetic field with a central spacer in the shimming gap and the dashed line without the central spacer. In the figure are also shown the radial distributions of gap lengths.

Figure 2–3 shows the azimuthal distributions of the magnetic field at 300 mm, 400 mm, and 470 mm of radius. The exciting current is 120 A and 70 A respectively. Without magnetic shimming, as shown by a dashed line, the field distribution shows the strong component of the first harmonics and the effect of three pillars. This effect can be explained by the fact that the material of pillars is not magnetization free perfectly and further by the fact that the azimuthal gap length distribution are in its maximum at the position of pillars. As shown by a solid line in Fig. 2–3, the first harmonics component in the azimuthal distribution is reduced to within 1 gauss irrespective of the exciting current when the magnetic shimming is performed. Shimming plate was placed in the upper shimming gap only, to correct the magnetic median plane, determined by a floating loop method, to coincide with the mechanical median plane of the magnet. The shape, position, and thickness of shimming plate are shown in Fig. 2–4.

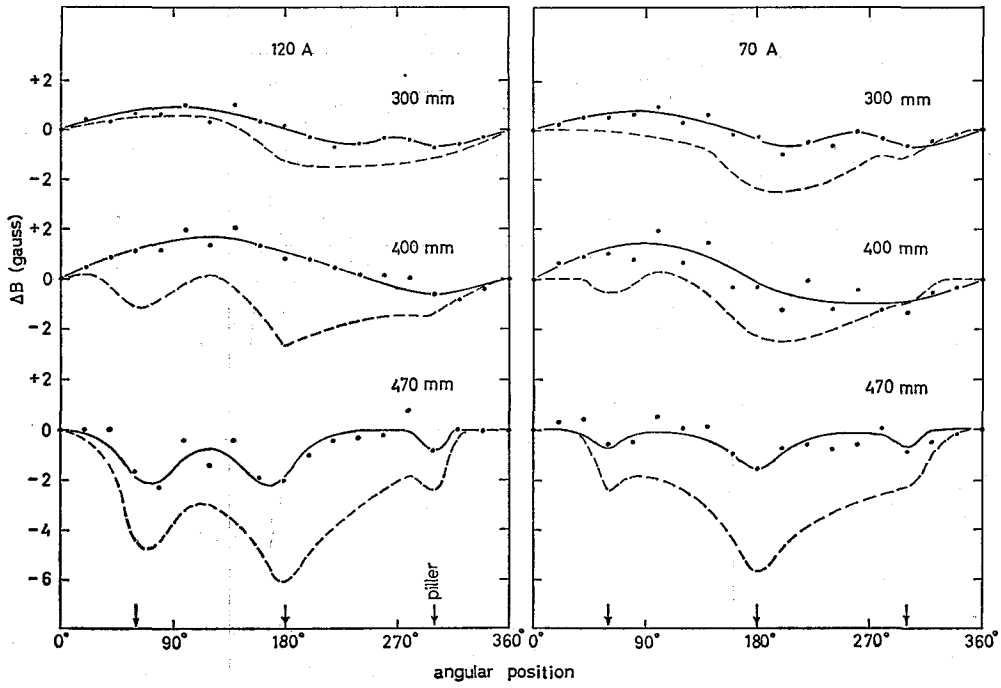

Fig. 2–3. The azimuthal distributions of the magnetic field at radius of 300 mm, 400 mm, and 470 mm. The exciting current is 120 A and 70 A.

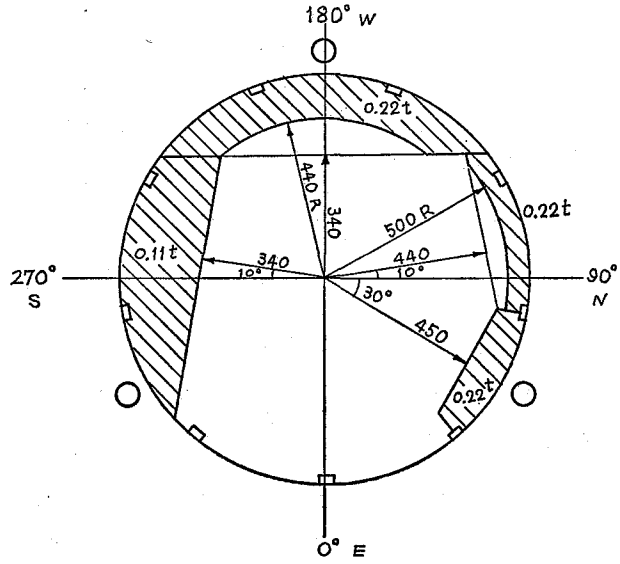

Fig. 2–4. Shape, position, and thickness of shimming plate.

III. VACUUM SYSTEM

The structure of the vacuum system were decided taking the following principles into account.

1) The vacuum acceleration chamber should not use the pole tips as lids like in the old cyclotron and should be feasible even if the pole tips are replaced with new type ones.

2) The vacuum acceleration chamber should be demountable without the decomposition of the main magnet.

3) The Q value of the whole vacuum system should be so small that the He (3) gas could be used repeatedly.

4) The pressure of the vacuum chamber should be less than a few times 10^{-6} Torr, and the evacuation time constant should be of the order of one second.

The plan view of the arrangements of the vacuum chamber, resonant line and the vacuum pumps is given in Fig. 5–1 in later section. The vacuum acceleration chamber is constructed so as to surround the magnet poles. The chamber consists of one top plate, one bottom plate, six rectangular posts and three pieces of vertical walls. The open end of the chamber is coupled to a box of which the explanation is given later. All parts of the acceleration chamber are made from non magnetic stainless steel (SUS27).

The weight of the acceleration chamber is supported by four stands attached to the lower side coil tank of the main magnet and by two posts set on the floor.

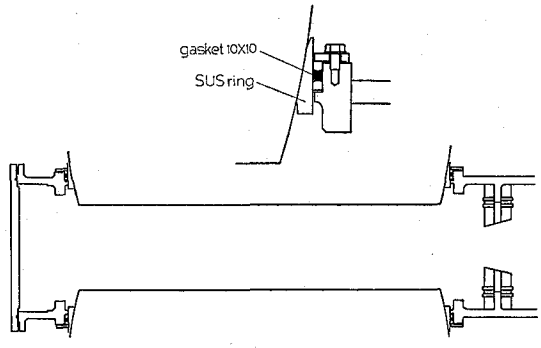

Fig. 3–1. Vacuum sealing of the top plate to the magnet pole.

Figure 3–1 shows the vacuum sealing method of the top plate to the magnet pole. A ring made from SUS27 is fixed to the magnet pole with epoxy resin, and then the opening of the top plate are coupled to this ring tightly via rubber gasket of $10 \times 10\ mm^2$ cross area.

To keep the leak tightness at the corner of the chamber, rubber gasket to rubber gasket contact method is adopted. Details of this sealing method are shown in Fig. 3–2. The fitting of the gasket to gasket is adjusted by two screws as shown in the figure.

Inter coupling box is made from copper. This box is drum shaped and has three holes. A hole on the west side of the box is of rectangular shape and is connected to the

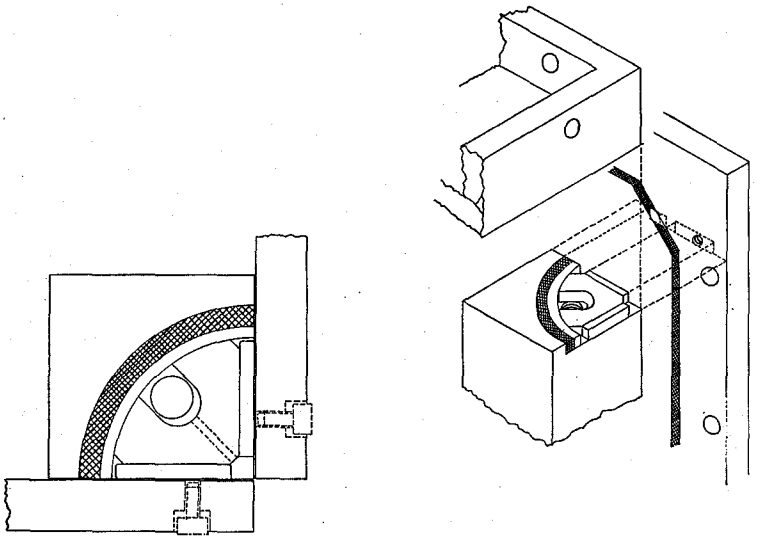

Fig. 3–2. Three way sealing method at the corner of the vacuum chamber.

opening of the acceleration chamber leak tightly. A hole on the east side of the box is of a circular shape and is connected to the outer shell of the co-axial line. On the body of the box, 18 holes of rectangular shape, $32 \times 580\,mm^2$, are cut over half circumference. The conductance of these holes amounts to 30,000 *l*/sec. Parallelepiped envelope covers this semi-circumference and is connected to the evacuating system.

Co-axial resonant cavity consists of outer shell and inner shell. The outer shell is made from oxygen free copper and re-inforced with steel frames. Thickness of the wall is 18 mm in average. Inner wall of the cavity is machined to 5 μm surface roughness and to the diameter of 1,200 mm. The inner shell is also made from oxygen free copper. Its outer diameter is of 400 mm and is also machined to 5 μm surface roughness. This copper pipe is supported with a stainless pipe as described in section V.

To avoid hidden spaces to be evacuated, screws used to fix various parts inside the vacuum are all drilled along their axes and copper liners which cover the pole tip surfaces and vacuum chamber plates are bored with holes of various diameters.

The volume to be evacuated was estimated as 4700 liters and the surface area as $4 \times 10^5 cm^2$. Tolerable leak and outgassing rate from the surface area was estimated as 0.3×10^{-3} Torr *l*/sec and 0.8×10^{-3} Torr *l*/sec respectively. Main oil diffusion pump of 22 inches diameter was selected to maintain the pressure in the acceleration chamber less than 2×10^{-6} Torr. Its nominal pumping speed is 10,000 *l*/sec. To use this diffusion pump as an evacuating system of the cyclotron, special cautions are paid; a helium leak detector is equipped at the top of the buffle, freon refrigerator was equipped to cool down the buffle and the top nozzle of the diffusion pump was placed inside the buffle. It was a trial to use the helium detector in this position, and experience shows that the sensitivity of the leak detection is of the order of 10^{-6} Torr *l*/sec. The operation characteristics of this pump is shown in Fig. 3–3. Four peaks as indicated by arrows in the figure indicate the starting point of the activity of four nozzles. 4.2 *l* of LION S oil is used in this pump.

Figure 3–4 shows a block diagram of the cyclotron evacuating system. One booster oil diffusion pump and four mechanical pumps are used as a fore pump and

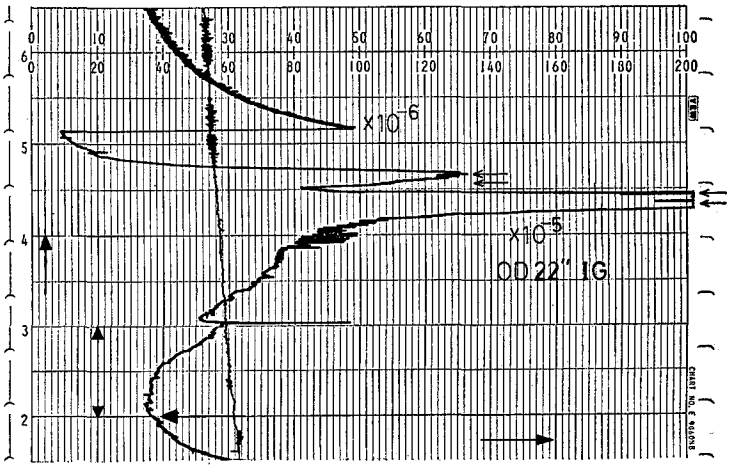

Fig. 3–3. Characteristics of 22 inches oil diffusion pump. Four arrows indicate the starting points of the activity of four stage nozzles. The speed of the flow chart is 10 min./Div. The arrow at the horizontal line of 2 shows the starting point of the pump heater.

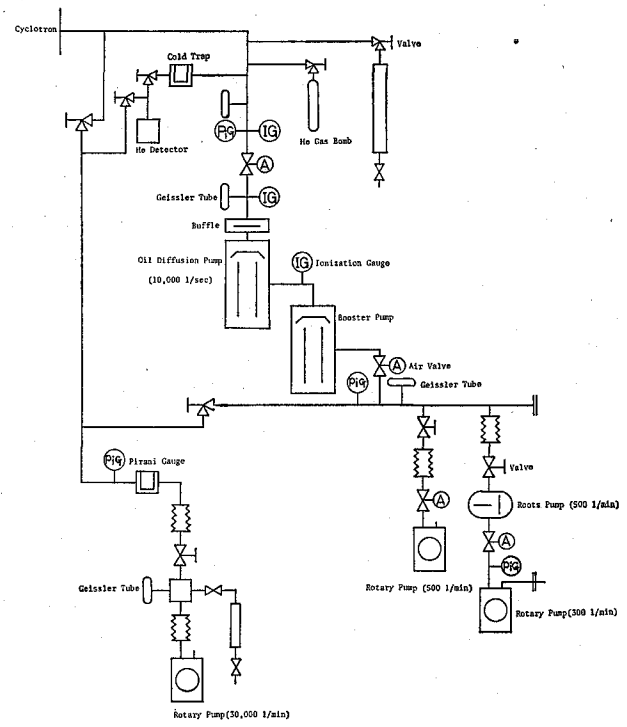

Fig. 3–4. Block diagram of the evacuating system. The pumping speed of the left side rotary pump should be read 3,000 *l/min.*, and that of the middle rotary pump should be read 300 *l/min.*

roughing pumps respectively. One of these mechanical pumps is a rotary pump of 3,000*l*/min pumping speed and is used for the preliminary evacuation of the cyclotron. Another rotary pump of 300 *l*/min pumping speed is used in normal operation of the cyclotron. When the ^{3}He ions are accelerated, a roots pump of 500 *l*/min pumping speed and a rotary pump of 300 *l*/min are used in series to re-circulate the ^{3}He gas.

Ionization gauge to measure the pressure of the acceleration chamber is set at a magnetic field free space via a stainless steel pipe of 2.0 meters long and of 41 mm diameter. Due to the conductance of the pipe, the indication of the vacuum gauge is about twice of that of the chamber.

The leak from cooling pipes inside the vacuum system was tested with an air bubble method beforehand the system was constructed. Details of this leak hunting method are reported in Ref.[3)]

After closing the leak from the cooling pipes and the leak of the vacuum acceleration chamber was tested separately, whole system was constructed and the leakage was hunted by evacuating the system. Three months of leak hunting were needed to get the desired pressure. From atmospheric pressure to 10^{-3} Torr, propane gas was used as a probe gas and a pirani gauge indicated the rise of partial pressure of propane gas leaked. From 10^{-4} Torr to 10^{-5} Torr also the propane gas was used to detect the leakage, but this time an ionization gauge was used as an indicator. From 10^{-5} down to 10^{-7} Torr, helium gas was used as a probe gas and the helium leak detector was used as an indicator. At present, Q-value of the sytem is 4×10^{-4} Torr *l*/sec and the final pressure of the chamber is 2×10^{-6} Torr.

IV. COOLING SYSTEM

Figure 4–1 shows a block diagram of the cooling system. The system is divided into six groups. Group 1 is in charge of the cooling of the main magnet. This system is the same as in the old cyclotron. Group 2 is in charge of the cooling of the oscillator power tube. City water is used to cool directly the main power tube of the oscillator. Group 3 deals with the cooling of the dee, dummy dee, lining plates, inter coupling box and co-axial resonant cavity. Purified water is used as a coolant. The inlet pressure is 5 kg/cm^2. The flow rate in the cooling pipes was calculated and the number of pipe lines was decided so as to give 5°C rise when the power lost in these systems amounts to 120 kW, that is, the full output power of the oscillator. To cool the outer shell of the resonant cavity, three lines of cooling pipes of 12mm diameter are soldered to the outer surface of the cavity. Caution was paid to cool its flange. The cooling water of the inner shell flows spirally through the gap between the inner surface of the shell and the outer surface of the stainless steel tube which supports the inner shell. The inter coupling box is cooled from outside by five lines of cooling pipes of 12 mm diameter. Cooling pipes of the dee and the liner are welded to the reverse side surfaces. Caution was paid to cool the front edge of the dee and the place of the liner just above and under the edge of the dee. As mentioned in section VII, since full power output of the oscillator is unnecessary to produce dee voltage of 100 kV, which is the value of dee voltage of usual operation of the cyclotron, the cooling of the heat generated by the R.F. oscillation is sufficient. As a result, the large frequen-

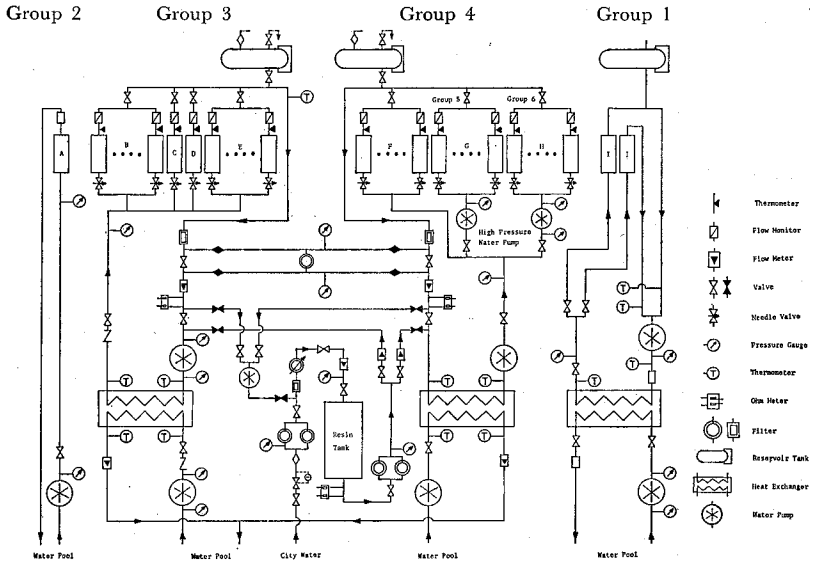

Fig. 4–1. Block diagram of the cooling system.
A: Oscillator power tube B: Dee system
C: Dee stem (inner shell of the resonator)
D: Outer shell of the resonator E: Dummy dee, lining plates, coupling condenser, and frequency compensators
F: Evacuating system G: Ion source system
H: Deflector, beam probe, and phase selector I: Coil of main magnet

cy shift caused by thermal deformations in the case of old cyclotron does not occur in the new cyclotron. The frequency variation is less than 2 kHz at 13 MHz operation. Group 4 deals with the cooling of evacuating system. The inlet pressure is 2 kg/cm^2. Groups 5 and 6 are subgroups of 4 and group 5 is in charge of the ion source cooling and group 6 the deflector, beam current probe and phase selector. Two high pressure water pumps connected to a pipe line of group 4 pressurises a purified water to 10 kg/cm^2 and used in groups 5 and 6. Details of the ion source cooling is described in section V.

As seen in Fig. 4–1, the whole cooling system is a closed, re-circulating system. Heat generated at every part of the cyclotron is delivered finally to the city water of 400 m^3 in the water pool. The temperature rise of this stored water is about 4°C per one day operation of the cyclotron. When a long-term operation of the cyclotron is necessary, the heat conserved in the water pool is released by a cooling tower coupled to the water pool.

The number of cooling lines amounts to about 100, which accords to the number of parts to be cooled. At each inlet of the cooling lines, a needle valve is set to adjust the flow rate of water. At each exit is coupled a specially disigned flow monitor and a thermometer in series. The structure and the characteristics of the flow monitor are shown in Fig. 4–2. This flow monitor is made from transparent acrylic acid resin. CdS element, small piece of brass cylinder inside the flow monitor and a small lamp are composed to detect the shut down of the water flow. Figure 4–3 shows the block

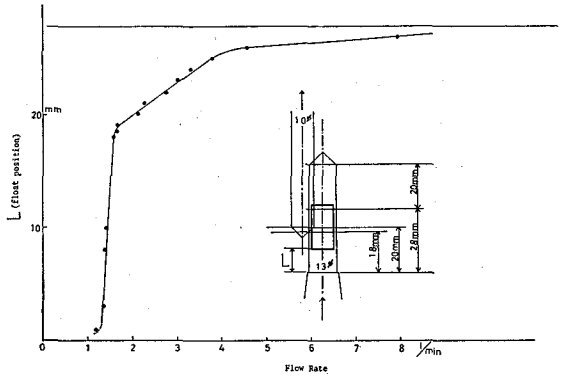

Fig. 4–2. Structure and characteristics of flow monitor.

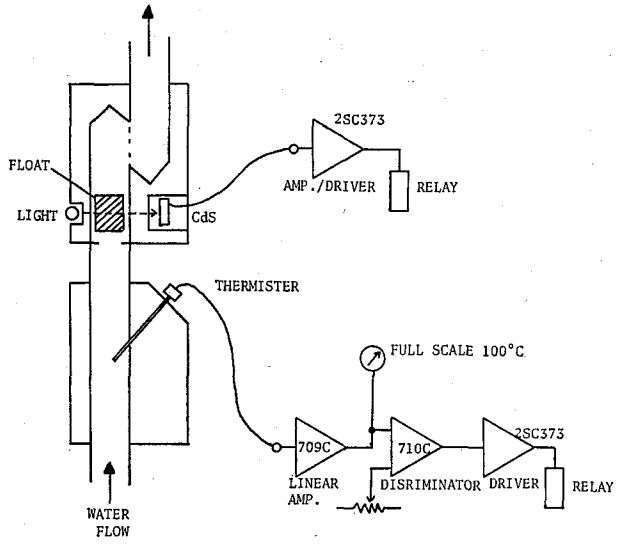

Fig. 4–3. Block diagram of the electric circuit to detect the position of the brass cylinder in the flow monitor.

diagram of the electronic circuit to detect the flow rate. Even if the cyclotron area is not dark, the signal obtained is sufficient to interlock other devices.

In the case of the old cyclotron, the removal of air bubbles in the water was a necessary task beforehand the operation of the cyclotron and several hours were needed every time the water was filled. To avoid this work, two water reservoirs of 50 *l* of each capacity are set at the highest position of the cooling system of group 3 and group 4 to exhaust air bubbles.

V. ACCELERATION SYSTEM

V.1. Dee, Dummy Dee and Resonant Cavity

The plan view of the arrangement is shown in Fig. 5–1. To make the extraction of the beam easier, the angle of the front edge of the dee was selected to be 80° with respect to the direction of the dee stem axis. The relative direction of the dee stem

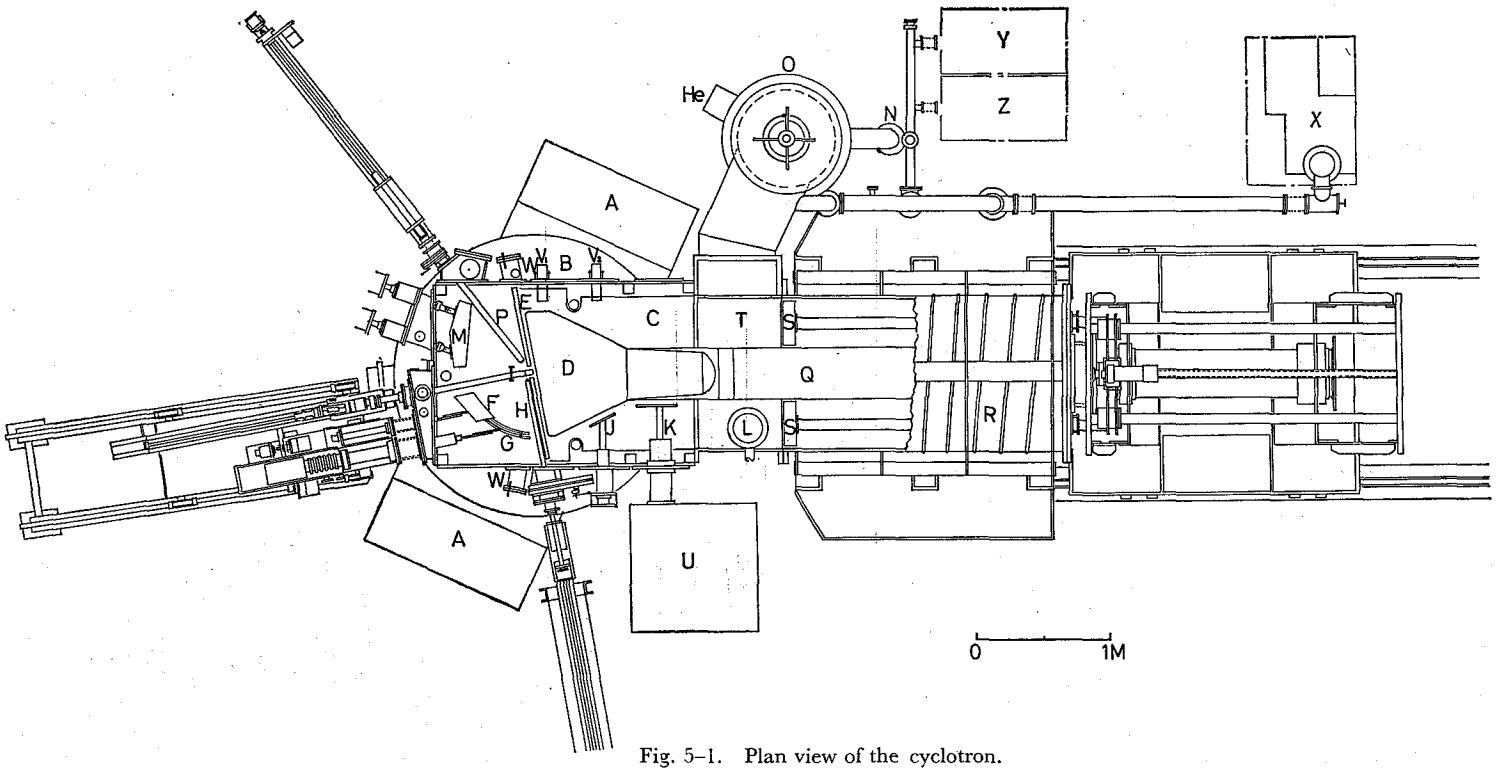

Fig. 5–1. Plan view of the cyclotron.

A : Main magnet B: Coil tank of magnet C: Vacuum chamber D: Dee E: Dummy dee
F : Septum G: Deflector H: Phase selector I: Ion source J: Capacitance compensator
K : Coupling condenser L: Inductance compensator M: Magnetic channel N: Booster diffusion pump
O : Main diffusion pump P: Beam probe Q: Dee stem R: Outer shell of the co-axial resonant cavity
S : Shorting plate T: Inter coupling box U: R. F. Oscillator V_1, V_2: Voltage pick up condensers
W: Window X: Rotary pump (3,000 *l*/min.) Y: Roots pump and rotary pump Z: Rotary pump (300 *l*/min.) He: Helium leak detector

axis to the direction of the main magnet center line is the same as in the old cyclotron, therefore, the angle between the direction of the dee front edge and the direction of the magnet yoke is 35°.

The distance between the dee and the copper liner of the pole tip is decided to be 42.5 mm taking into account that the necessary dee voltage is 100 kV. Experience showed that 120 kV driving is possible. Especially the cooling of the front edge of the dee and the dummy dee was taken into account to reduce the probability of discharge. The inner gap length of the dee is 22 mm, and the separation distance between the dee and the dummy dee is 20 mm. To avoid the twisting of the dee plate, copper frames fixed to both side-edge of the dee are connected with a copper frame with each other and then fixed to a big frame made from stainless steel rigidly so as to define the plane of the dee. The dee constructed as a whole is bolted to the dee stem, which is the inner shell of the co-axial resonant cavity. The electric contact between the dee stem and the rear end of the dee is done with four quadrant copper ring. The edge of the ring is of a wedge shape and fitted by screw to both ends of the shell and dee.

Figure 5–2 shows the schematic structure of a puller which is attached to the front edge of the dee. The effect of this puller on the ion acceleration is discussed in section VII.

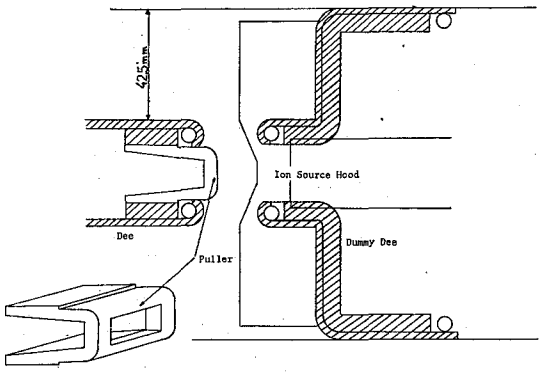

Fig. 5–2. Shematic structure of the puller.

Liners which cover the pole tips and the side walls of the vacuum chamber are elongated to the inside of the inter coupling box and are bolted to the inner surface of this box. To make a good electric contact between the edge of this box and the edge of the outer shell of the co-axial resonant cavity, small groove was machined at the edge of the cavity and a silver wire of 1.5 mm diameter was embedded in this groove. Leak tightness of the coupling is held by a rubber gasket just outside the silver wire. Since the first time construction of the new cyclotron, the coupling was disconnected several times up to the present, but no trouble occurred about the electric contact.

The inner diameter of the resonant cavity is 1,200 mm, its length 2,200 mm and the outer diameter of the inner shell is 400 mm. The effective length of the co-axial resonant cavity is varied by changing the position of the shorting plate. To make good electric contact between the outer shell or inner shell of the resonant cavity and the shorting plate, a contact device as shown in Fig. 5–3 was designed. 16 pieces of copper block are used for the contact between the inner shell and the shorting plate

and 48 pieces for the contact between the outer shell and the shorting plate. 4 pieces are grouped together and are pressed to the surface of the shell by a combination of pressurized air (2 kg/cm^2), a bellows and levers. A piece of silver wire of 1.9 mm diameter is embedded at the top of each block and several sheets of copper foils conduct the electric current and the heat in parallel from the contact device to the shorting plate. The contact resistance measured was 0.1 mΩ or less and the heat generation was not observed.

The components of the cavity are mounted separately on two four-wheel trucks. One truck supports the outer shell and the other end plate of the cavity, driving mechanism of the shorting plate and the dee stem. The dee stem is supported at two points to adjust the posture of the dee. Wedge shaped couplers are equipped and a male coupler of the truck is caught by a female coupler fixed to the floor when each truck goes forward. These couplers serve to secure the reproducibility of relative positions of the dee and the resonant cavity within 0.2 mm.

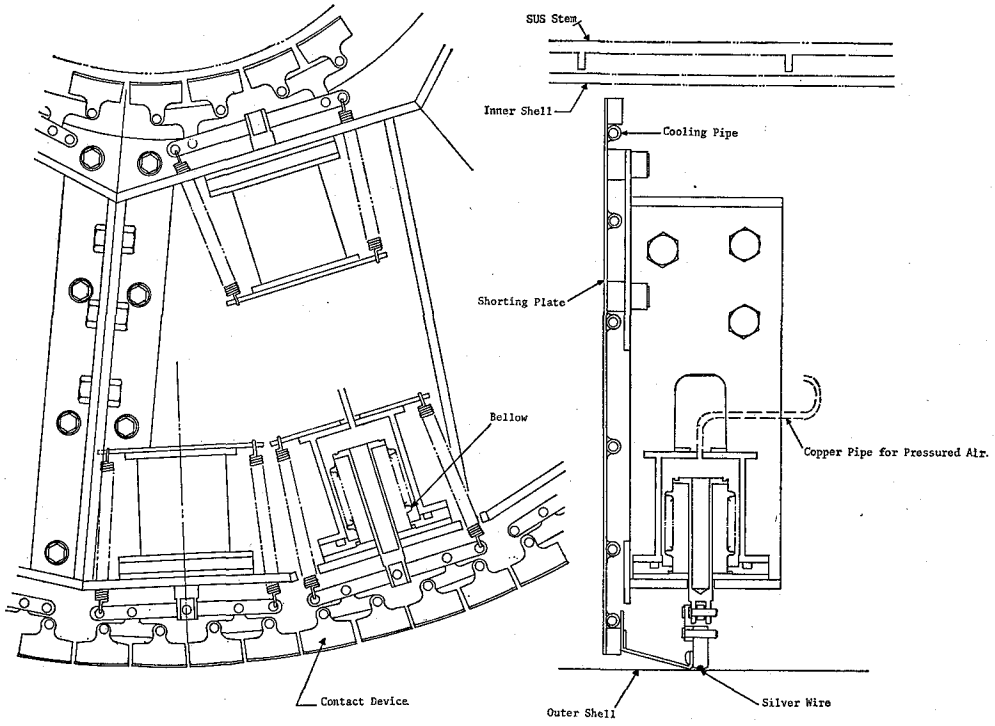

Fig. 5–3. Contact device of the shorting plate.

The frequency of a quarter-wave mode oscillation of this resonant system ranges from 10 to 19 MHz. Its Q value was estimated at several value of frequencies and was 10,900 at 10 MHz. Detailed characteristics of the R. F. oscillation are described in the preceding article in this Bulletin.

V.2. Ion Source

A cross sectional view of the front part of the ion source is shown in Fig. 5–4. Dual arm system was designed to fix the hood of the ion source. The direction of the

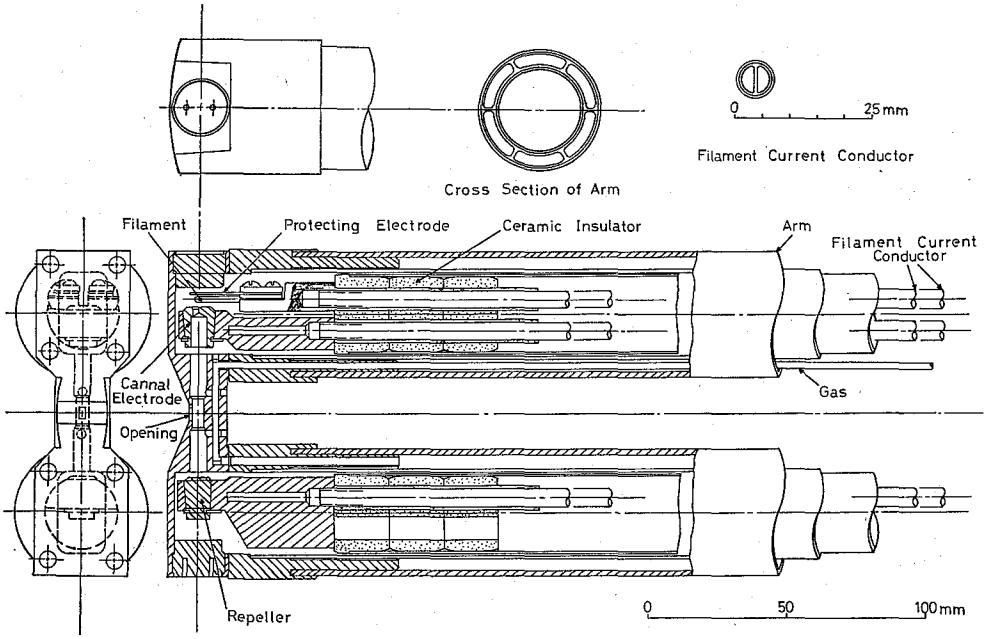

Fig. 5–4. Cross sectional views of the front part of the ion source, the arm of the ion source and the filament support.

arms is normal to the direction of the front edge of the dee and aims at a point 20 mm to the north from the center of the magnet. The dual arm are mounted on a brass slide which can move on a steel bed. When necessary, the total system of the ion source can be extracted from the acceleration chamber. See Fig. 5–1. The hood is made from molibdenum and is connected to the arm which is cooled by purified water. The opening of the hood is of rectangular shape of 4 mm hight and 2.2 mm width. The filament is of a hair pin type and is made from tungsten wire of 2 mm diameter. This shape is the same as that of the ion source of the old cyclotron. The power supply of the filament has a capacity of 6 V and 300 A of d. c. current. The filament current is kept constant independent of the state of the filament with a stabilizing circuit. The power supply of the accelerating electrode has a capacity of 300 V × 5 A plus 500 V × 1 A. A protecting electrode made from tungsten is set just above the filament and is fixed to one of the filament terminal plates. Accelerating electrode of electrons is of a canal shape and is set about 1 mm apart from the filament. The canal electrode is made from tungsten and is embeded in a copper block. This copper block is connected to a pair of copper tubings which are supported by ceramic insulators in the lower half of the copper tube of 28 mm diameter.

The repeller of electrons is set at the bottom of the hood and can be used as a melting pot of materials when necessary. The conductor of the filament current consists of a pair of three copper tubings. Two special type tubings of which the cross section is a semi-circle, are combined and inserted into a circular pipe of 6 mm diameter. Water flows in and out through these semi-circular tubings and cools down the terminal plate of the filament. The cross sectional view of these pipes is shown also in Fig. 5–1. These two conductors are supported by ceramic insulators and these insulators are

set in the upper half of the copper tube of 28 mm diameter. Gas inlet route into the hood is shown also in Fig. 5–4. The diameter of the route is 2 mm.

Each arm of the ion source consists of double coaxial copper tubings and six sector shaped tubings. The outer tubing is of 45 mm diameter and the inner tubing of 30 mm diameter. Six tubings of sector-shaped cross section are inserted into the space between the outer and inner tubings. The combination of these tubings are also shown in Fig. 5–4. To cool down the arm, water flows into three of six sector-shaped tubings and comes out from the remaining three.

A potential difference is applied between the filament and the canal electrode. To produce ions of gaseous elements, the hood and the canal electrode are grounded and the potential same to that of the filament is applied to the repeller. On the other hand, the potential of the repeller can be made positive to that of the filament when the repeller is used as a melting pot of heavy, solid elements.

The flow rate of gases for the ion source is adjusted by a needle valve, which was the one used in the case of the old cyclotron. Gases of hydrogen, heavy hydrogen and helium 4 are supplied from bombs set in the operation room. Figure 5–5 shows the gas supplying circuits of the ion source.

The characteristics of the ion source was studied by measuring the beam current at the radius of 47 cm, which is the radius of maximum acceleration. Figure 5–6 shows the beam current of H_2^+ ions as functions of arc voltage, that means the accelerating potential of electrons, when the gas flow rate is varied. As seen from Fig. 5–6, the beam current saturates at about 70 V of arc voltage irrespective to the gas flow rate. Filament current is kept constant at 210 A in this case. Figure 5–7 shows the beam current as a function of gas flow rate, where the arc voltage and the arc cur-

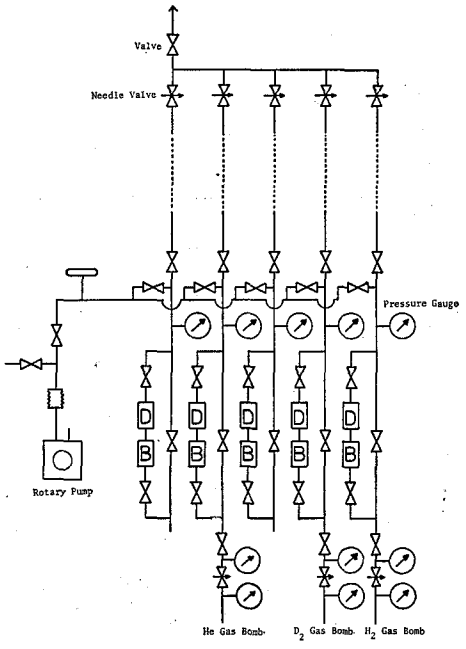

Fig. 5–5. Block diagram of the gas supplying circuit.
D: Desiccator (silica gel) B: Bubble flow monitor.

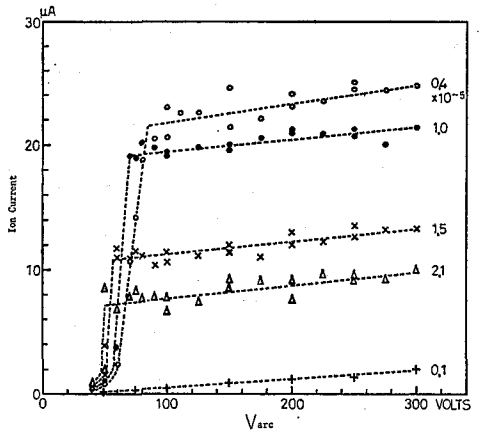

Fig. 5–6. Relation between the beam current and the arc voltage. The gas flow rate are shown at the right hand side and the unit should be read 10^{-6} Torr..

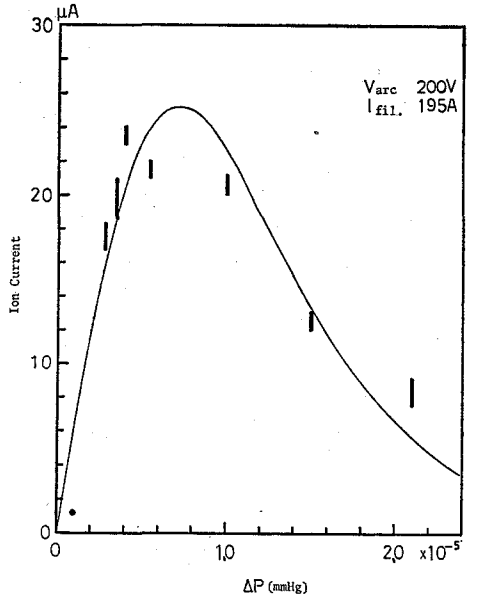

Fig. 5–7. Relation between the beam current and the gas flow rate. For the solid line, see text. The order of the abscissa should be read 10^{-6}.

rent are fixed. Figure 5–8 shows the beam current as a function of the arc current. Solid lines in Figs. 5–7 and 8 are calculated curves to fit the experimental results. The calculation is based on the assumption

$$I \propto pqe^{-\alpha pL}/(\alpha p+\beta qe^{-\alpha pL})$$

where p is the gas flow rate, q the arc current and L the distance between the accelerating electrode and the center position of the hood and L is 38.5 mm in this case. The relation above mentioned is derived easily from the following considerations:

(1) Number of ions produced in the hood is proportional to the electron current and to the gas pressure inside the hood.

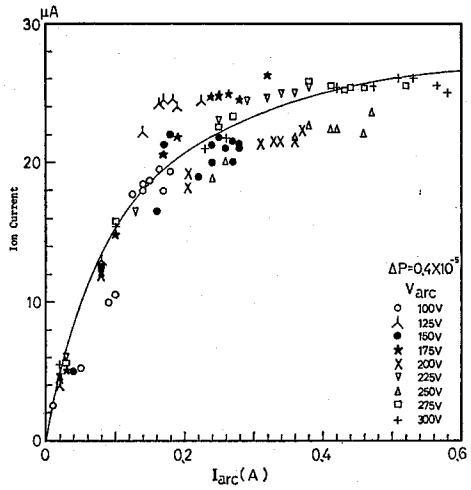

Fig. 5–8. Relation between the beam current and the arc current. For the solid line, see text. The order of the gas flow rate should be read 10^{-6} Torr..

(2) The electron current is proportional to the arc current and is an exponentially decreasing function of the gas pressure.

(3) Ions are lost by the scattering on neutral gas molecules and are lost also by the recombination processes.

α and β in the equation are the parameters to fit the curve to the experimental results and there is a relation

$$\frac{1}{\lambda}=\alpha\times p.$$

From the figures, the most relevant value of α satisfies the relation

$$\frac{1}{\lambda}=0.18,$$

where λ is the mean free path of electrons in the gas. Gas flow rate is adjusted by measuring the pressure rise at the head of the vacuum pump. Under normal operating condition, the pressure rise $\Delta p=0.4\times10^{-6}$ Torr, therefore the gas pressure inside the hood is estimated to be about 2 Torr.

V.3. Beam Current Probe and Phase Selector

The beam current probe is located at the beam exit of the vacuum chamber as shown in Fig. 5–1. It moves along radial direction and detect the beam current at any radius. Two types of current probes, *i.e.*, a differential type and an integral type, was prepared. Figure 5–9 shows the structure of these current probes. The probe is fixed to a slide outside the vacuum chamber and this slide is moved by a remote controlled motor.

To select the beam of relevant phase and to reduce the unnecessary beam loading, a phase selection device was designed. Figure 5–10 shows the structure of this phase selector. The phase selector consists of two arms, *i.e.*, upper and lower arm. On the front of each arm, a reed of 6×9 mm^2 cross area is equipped. This reed can be rotated

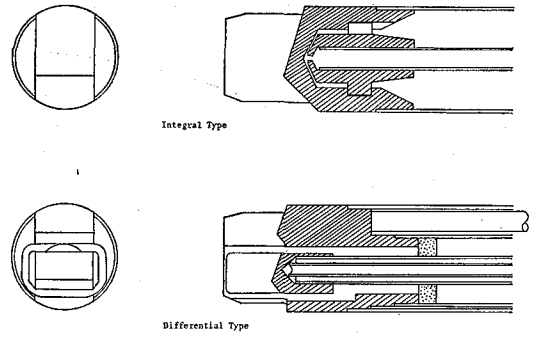

Fig.5–9. Cross sectional veiws of the front part of beam probes.

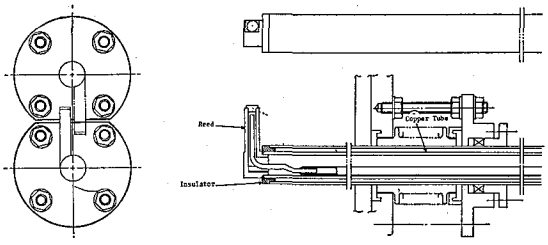

Fig. 5–10. Structure of the phase selector.

around the axis of the arm from outside the chamber. Each arm moves independently with each other and its direction is parallel to the front edge of the dee. The position relative to the dee or to the dummy dee is shown in Fig. 5–1.

V.4. Deflector and Magnetic Channel

The beam deflection system is inserted to the chamber through the west side wall. Its position in normal operation is shown in Fig. 5–1. The profile of the deflector was designed so as to match the beam orbit. The beam orbit was calculated under the conditions that the field gradient $dV/dr = 100$ kV/cm, the deuteron beam of 15 MeV reaches to the entrance of the deflector and the magnetic field is that given at exciting current of 123 A. The beam orbit and dimensions of the deflector are shown in Fig. 5–11.

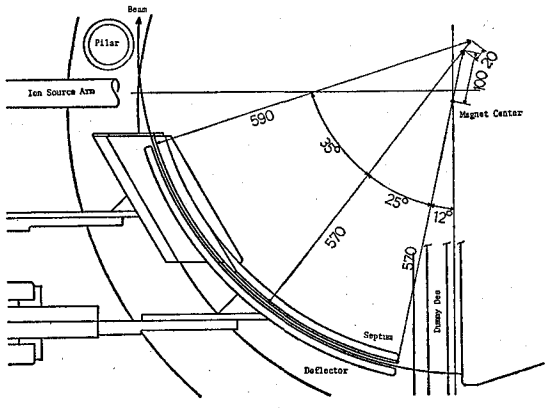

Fig. 5–11. Dimensions of the deflector.

The septum electrode consists of 17 pieces of tungsten plates which are fixed to a copper frame by screws. This copper frame is placed upon the liner of the pole tip. The position of this frame, therefore, that of the septum, can be varied from outside the chamber by moving a rod fixed to this frame. The deflecting electrode is made from copper. Also the position of the deflecting electrode can be varied from outside the chamber by moving a rod fixed to this frame. This rod is insulated electrically with a ceramic insulator of long nozzle shape. The rod of the septum electrode and the insulator of the deflecting electrode are mounted on two slides separately and each slide moves on a bed. The direction of the bed axis can be changed manually in a limited range, therefore, the position of the deflector can be changed azimuthaly. These two beds, together with the bed for the ion source, are mounted on a four-wheeled truck. Further, a vacuum sealing box of the deflector system is also fixed to this truck. Then, the deflector system can be drawn out from the chamber by moving this truck. The potential of the deflecting electrode is supplied from a source of 100 kV × 10 mA capacity. High voltage generating part of this power supply are packed in an oil-filled tank.

To reduce the horizontal defocusing action of the magnetic field a magnetic channel was prepared after the manner developed in the Institute of Physical and Chemical Research.[4] Figure 5–12 shows the dimensions of the magnetic channel.

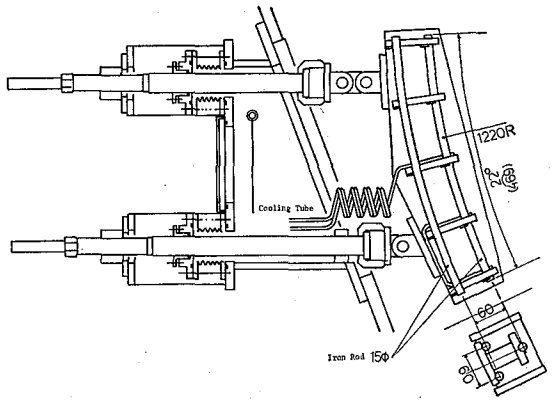

Fig. 5–12. Dimension of the magnetic channel.

VI. CONTROL SYSTEM

VI.1. General Description

In the design stage of the control system, special cautions were paid to satisfy the following conditions:

1. Both the central control system and the local control system should be prepared. The local control system has a superiority to the central system and the power sources of the components of the cyclotron are switched on by the local control system for the safety of the cyclotron operator.

2. The local control system is used to test each component of the cyclotron at its site.

3. To retain room for future improvement of the control system, coupling between local system and central system is performed via two pairs of junction boxes. One pair is used for the transfer of low voltage, low frequency signals for remote controls, and cable bundles covered by copper shield (CVVS) connect this pair. The other pair is used for the transfer of low level, high frequency signals, and coaxial cables connect this pair. Junction boxes in the cyclotron area should be shielded carefully to avoid the influence of the stray field of the cyclotron oscillator.

4. The central control system deals with limited, simplified operation of the cyclotron and it is desirable that one person operation of the cyclotron is possible.

5. The control system should be fool proof, and sequence order of switching on or off should be proved by relevant devices and interlocks.

6. Any component of the control system should be standardized, for example, NIM standard size is applied to all module panels to simplify the layout of the control console. Lighted push button switches are used to reduce the space, to indicate the sequence order and to make the operation of the control system easy.

7. Digital control system is preferable and the control system should be improved step by step to achieve the final form, that is, a computer regulated type and in that stage only a few parameters are left to be adjusted manually.

At present, the control system of the new cyclotron is far from final form, but precautions described above are almost satisfied and the troubles such as the wrong indication of meters due to the stray field of R. F. oscillation are not experienced.

VI.2. Details of Some Examples

In the following are described the functions of control circuits by taking some typical examples.

1. Figure 6–1 shows the block diagram of the arc current control of the ion source.

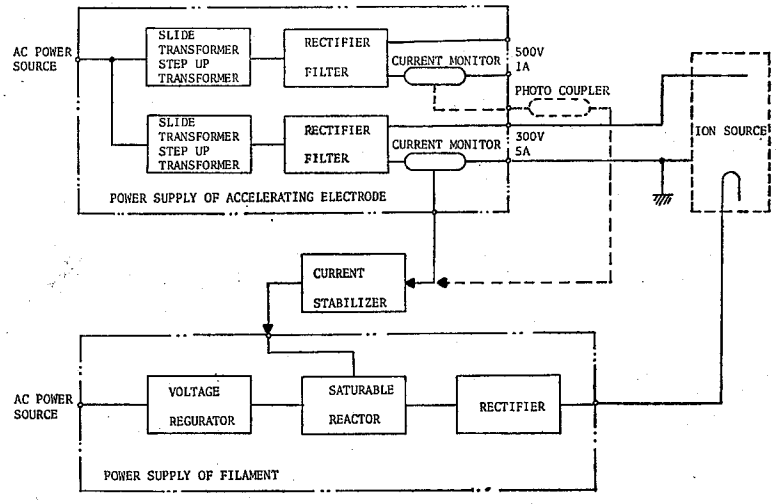

Fig. 6–1. Block diagram of the arc current control system.

The power supply of the accelerating electrode of the ion source consists of two sets of voltage sources. If two stage acceleration method is applied to the ion source, the potential at the monitoring resistor relative to the ground is too high to be used as an input signal of the stabilizer. In this case, a photocoupler is used between the resistor and the input of the stabilizer.

2. The vacuum tube control circuit of the old cyclotron magnetic field[1] was replaced by a new, transistorized circuit. Figure 6–2 shows this current stabilizer circuit. The parameters are selected experimentaly to avoid the hunting phenomenon. The error of current stabilization is less than 5×10^{-4}. The same circuit is used also for the beam analyzing magnet. The error is less than 3×10^{-4} in this case.

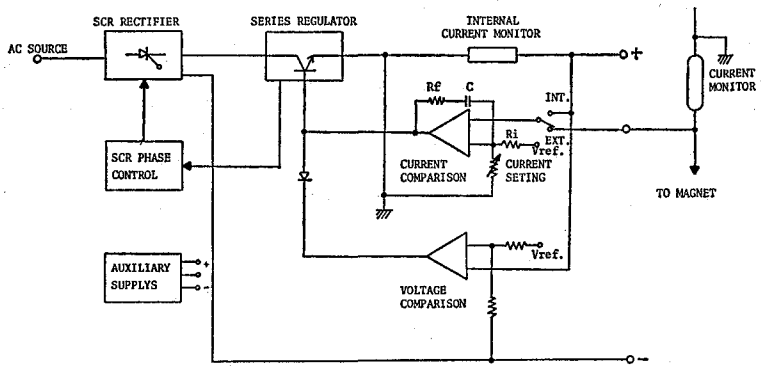

Fig. 6–2. Current stabilizer circuit of the main magnet coil.

3. Figure 6–3 shows the block diagram of the frequency stabilizer. The frequency is measured by a digital counter, 6 digits BCD output from the counter is compared to a fixed value of a digital comparator. The resulting error signal is used to drive the capacitance compensator. Two limiting switches generate signals of the over range drive of the capacitance compensator and then these signals are used to drive the inductance compensator.

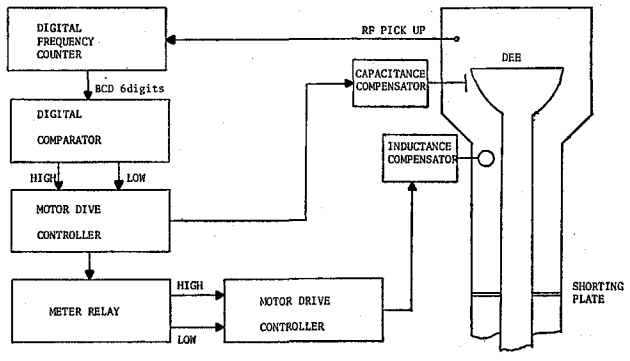

Fig. 6–3. Block diagram of frequency stabilizer. The word MOTOR DIVE in the third column of left hand side should be read MOTOR DRIVE.

4. Figure 6–4 shows the block diagram of the drive control system of the beam probe and so on. The direction and the speed of the motion of the probe can be chang-

ed remotely. Also the inertia of the driving motor is reduced by electronic circuit to stop the probe instantaneously.

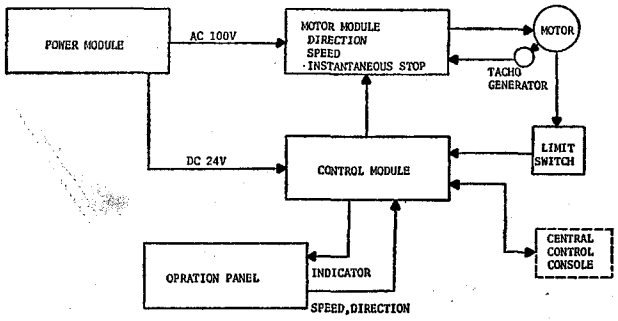

Fig. 6–4. Block diagram of the driving mechanism control.

5. The read out system of the position of the probe is a resistance and a Selsyn motor method and can measure the position within 1 mm. To read out the position with a sensitivity of 0.1 mm, the system shown in Fig. 6–5 is developed. This system consists of a gray coding plate, a photo mark sensor, an amplifier and a decorder–driver for a digital display tube and the revolution angle of the driving axis is measured digitly.

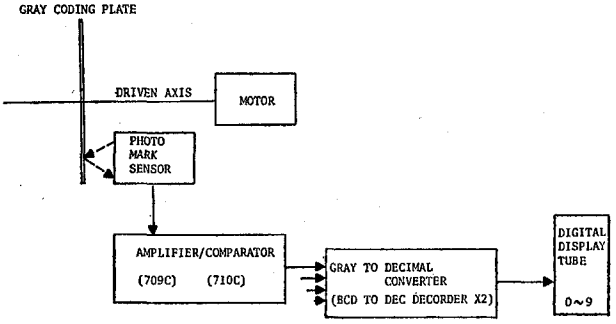

Fig. 6–5. Read out system of the position of probes.

6. Many kind of informations are necessary to operate the cyclotron and interlock system between these informations are needed to provide the means of orderly sequence control and alarming of failures. As an example, the control system of the R. F. oscillator is shown in Fig. 6–6. The switching order of each component is held fixed by the system as shown in the figure. Missoperation of the oscillator such as the switching on without cooling the power tube is prevented by a built-in interlock system. Signals from outside of the oscillator, that is, signals from entrances of the cyclotron area, from flow monitors, from vacuum gauges and from the power supply of the main magnet, interlock the operation of the oscillator.

Alarming signals informing that the cyclotron is in operation are also generated with this system to light the placards at entrances.

In the lower part of the figure is shown a flow chart of the automatic recovery

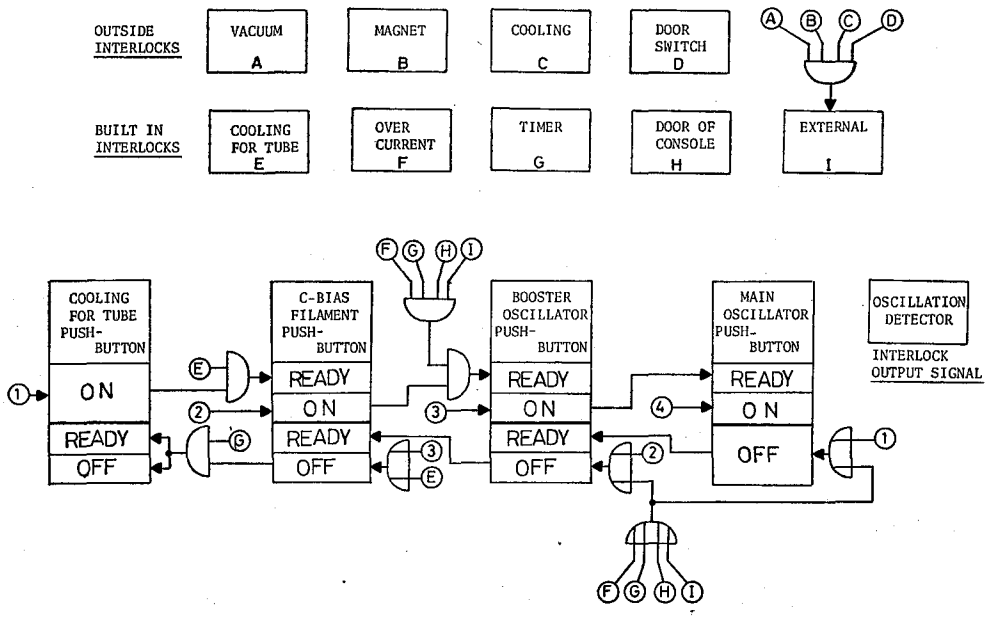

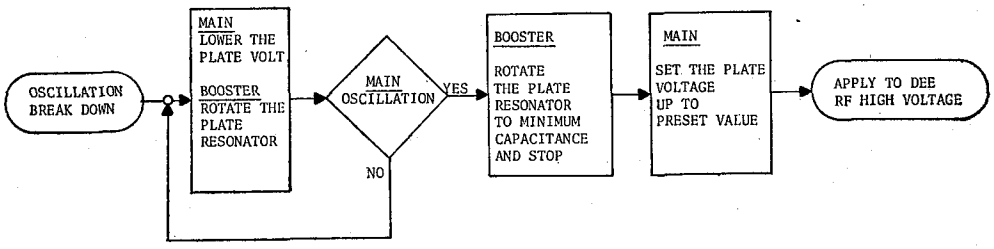

Fig. 6–6. Control system of the oscillator. Automatic recovery method of the oscillation is also shown.

method of the oscillation if it breaks down.

7. There are also informations which need the judgement of the operator. The operating conditions of the cyclotron should be adjusted manually based on the judgement. As an example, annunciator system is shown in Fig. 6–7. This system is used to indicate some troubles in the cooling system, the vacuum system, the oscillator system, and the deflector system. At the central control console, the operator is informed by a flicker light and a chime or a buzzer that a trouble occurred in some component system.

The resetable trouble in the deflector or in the oscillator system is alarmed by a chime. The break down of the vacuum or the failure of cooling system is alarmed by a buzzer. In this case, the local position of the trouble is indicated by a lamp at the local control console therefore the operator is called for to remove the trouble.

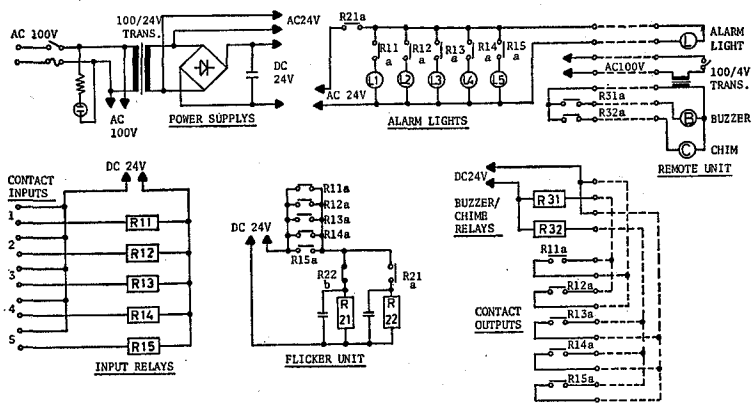

Fig. 6–7. Annunciator system of failures.

In conclusion, some remarks are given about the control system. 1. Experience showed that the high voltage feeding cable of the deflector was to be shielded to be free from the interference of the R. F. oscillation so as to get sufficient deflector voltage stability. 2. The shielding of signal cables and junction boxes was successful. As a result, the wrong indication of meters due to the stray field of R. F. oscillation is not experienced. 3. Sufficient cooling of each component of the new cyclotron is very important to assist the control system. In the case of the improved cyclotron, even in the free running mode, the frequency of oscillation and the dee voltage are much more stable than conjectured from the experience of the old cyclotron, and no manual control is necessary to operate the cyclotron.

Now, the control system can be divided into mutually independent subsystem of each component and no functional relations between each component should be taken into account. Therefore, automatic operation of the cyclotron is possible in the next stage.

VII. PERFORMANCE

VII.1. Beam Orbit in Central Region

The electric field distribution across the acceleration gap was calculated under the assumption that the dee and dummy dee are elongated to half infinity. Figure 7–1 shows the calculated results of the potential distribution along the median plane. The dimensions are shown also in Fig. 7–1. As seen in the figure, the potential drops nearly to zero at the position of the phase selector which is set at 60 mm apart from the center line of the acceleration gap. Figure 7–2 shows the electric potential distribution across the gap between the ion source and the dee in both cases where the puller exists or not. The calculation is also simplified under the assumption that the ion source, the puller and the dee are all half infinite.

Beam orbits in the central region were calculated in terms of the electric field distributions in Figs. 7–1 and 2 and the magnetic field distribution obtained experimentally. The magnetic field distribution is shown in Fig. 2–2. In this case, charge to mass

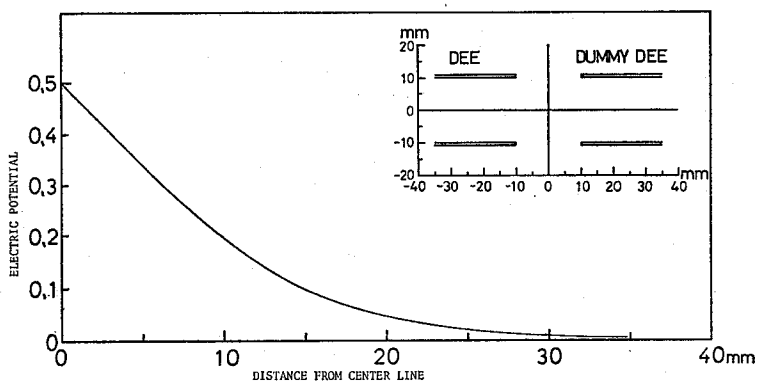

Fig. 7–1. Potential distribution along the median plane produced by half infinite dees.

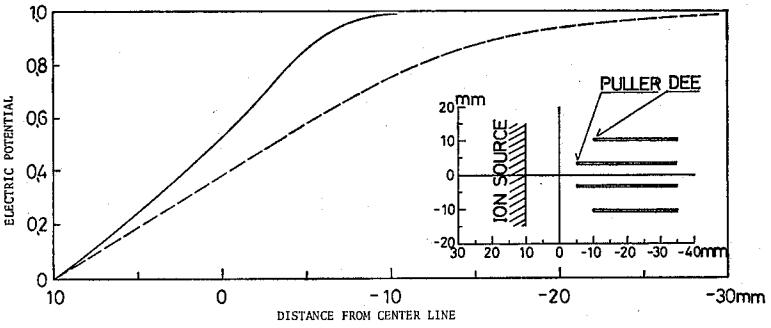

Fig. 7–2. Potential distribution near the ion source. The solid line represents the distribution when the puller exists. The broken line gives the distribution when no puller exists.

ratio of the ion is 1/2 and the dee voltage is assumed to be 100 kV. The result is shown in Fig. 7–3 for the first few turns of ions of which the phases at the starting point are assumed to be $+30°$, $0°$, and $-30°$ respectively. The phase angle is measured from

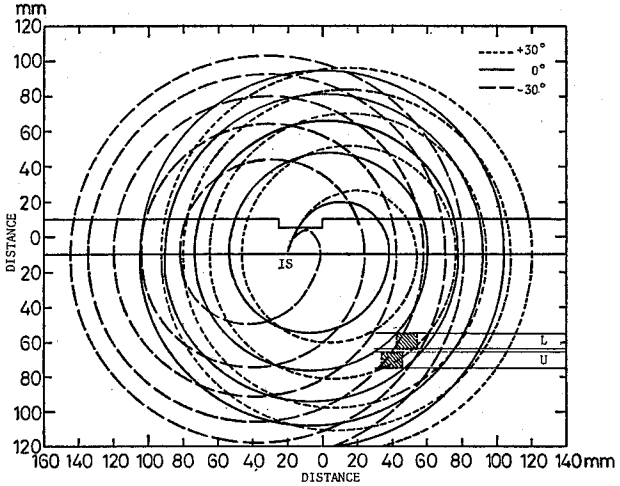

Fig. 7–3. Beam orbits in the central region.

the top of the R. F. potential. As seen in the figure, concentration of orbits occur in the front and rear of the ion source, but in contrary, after $n+1/2$ turns, where n is an integer, the orbits of different starting phases separate to each other and it is possible to choose some proper phase ions by the phase selector. If the phase selector is set at the position shown in the figure, ions of 0° and some neighboring phases can be accelerated further but ions of $+30°$ or $-30°$ phases are stopped. L and U in the figure mean lower and upper part of the phase selector and the shaded areas in the figure indicate the positions of the reed of the phase selector.

The scheme of ion acceleration was investigated by using the phase selector and a beam current probe. In Fig. 7–4 is shown the relation between a H_2^+ beam current at 45 cm radius and the position of the phase selector. The reed of the phase selector is moved parallel to the edge of the dee. The distance indicated on the abscissa of Fig. 7–4 is the same as in Fig. 7–3. The upper part of the figure shows the variation of the beam intensity as a function of the position of the upper phase selector. In this case, the reed of the lower phase selector is not used. The lower part of the figure indicate the effect of the lower phase selector. In this case, upper phase selector is not used. As seen from the figure, the beam orbit separation per turn is about 25 mm and this value agrees well with that seen in Fig. 7–3. The position of beam inhibition is different whether upper or lower phase selector is used. This is due to the fact that the upper phase selector moves 70.5 mm apart from the center line of the accelerating gap and the lower one 59.5 mm apart, and the beam strikes the reed of phase selector obliquely.

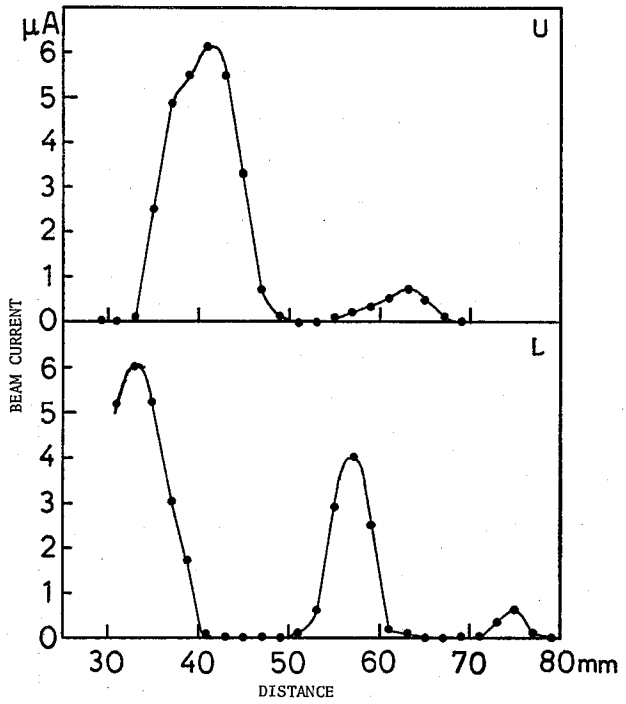

Fig. 7–4. Relation between the beam current at 45 cm radius and the position of the phase selector.

VII.2. Acceleration of Ions to the Maximum Radius

Figure 7–5 shows the vertical motion of the beam. This result is obtained from the following experiment. The beam current probe is set at 45 cm radius. The reed

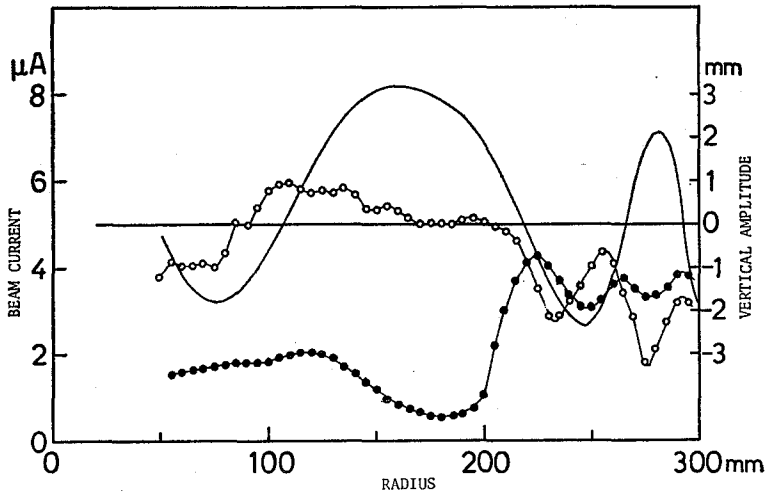

Fig. 7–5. The variation of the beam current at 45 cm radius when the upper or lower half of the beam are inhibited by the phase selector. For the solid line, see text.

of the upper or lower phase selector is turned on so as to cut the beam in the upper half or lower half space from the median plane. Then the variation of the beam current is measured as a function of the position of the upper or lower phase selector. The solid circles in Fig. 7–5 indicate the results when the upper half beam is cut by the phase selector and the open circles the results obtained when the lower half beam is cut. As seen in Fig. 7–5, the beam current at 45 cm radius varies its intensity slowly when the beam is cut in some radius less than 200 mm or so and then the beam intensity oscillates with a period of 50 mm.

Figure 7–6 shows the calculated vertical motion of a beam along the center line

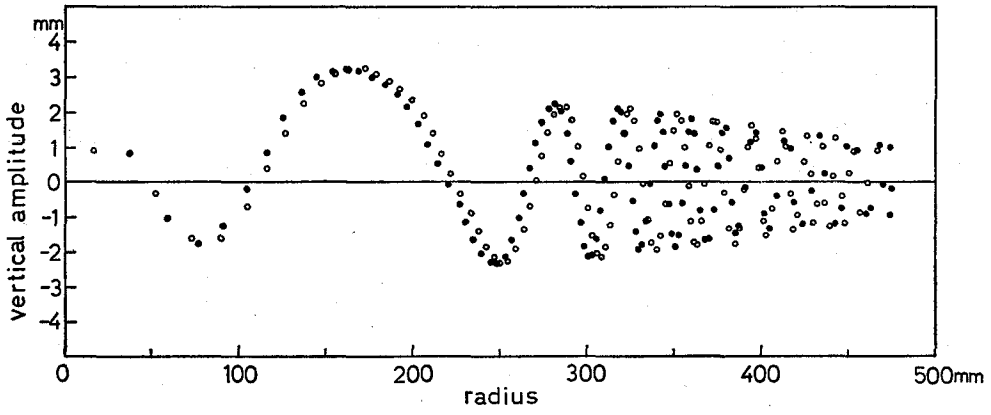

Fig. 7–6. Calculated results of the vertical motion of the beam started 1 mm above the median plane.

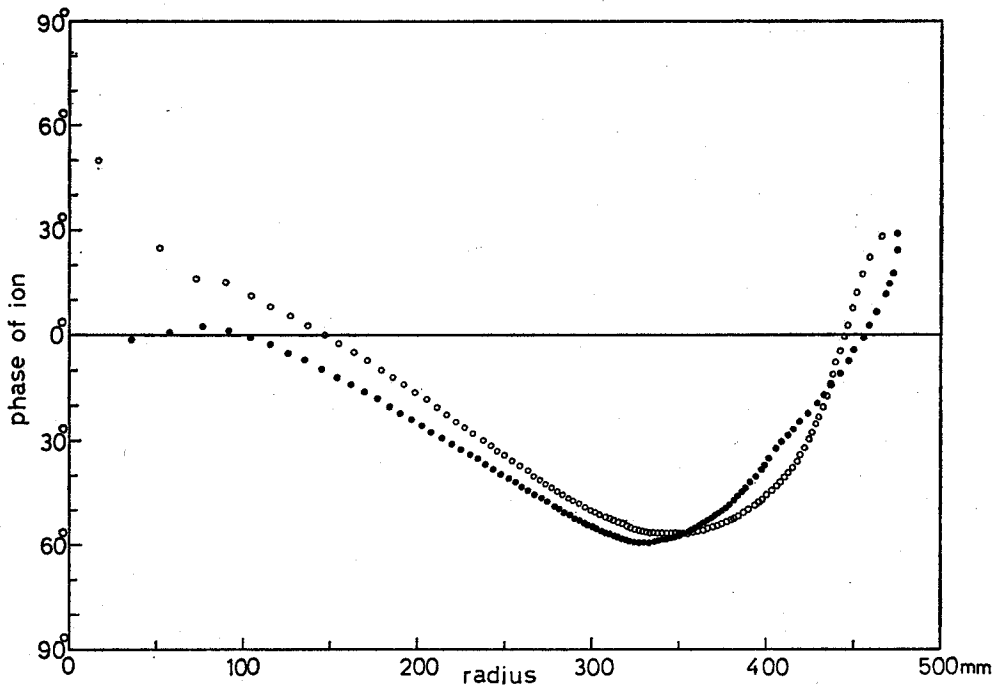

Fig. 7–7. Calculated results of the ion's phase to the accelerating potential at the center line of the accelerating gap. The open circles are the phase of ions at the north half of the accelerating gap. The solid circles at the south half.

of the acceleration gap. The calculation is done on the assumption; Ion source is located 20 mm apart to the north from the center. Ions start from the ion source with 0° phase to the R. F. oscillation and at 1 mm height from the median plane. The magnetic field is 17.081 kG at the center of the magnet, the R. F. frequency 13.00 MHz and the dee voltage 100 kV. Solid circles are for the beam which crosses the south side of the center line and open circles for the north side of the center line. Phases of the ions at the center line to the acceleration potential are shown in Fig. 7–7. In the figure, each circle corresponds to each crossing.

The solid line in Fig. 7–5 indicates a part of calculated results in Fig. 7–6. When compared in Fig. 7–5 the distribution of solid circles to the solid line, the correspondence between the current maximum and the ion displacement minimum is clearly observed. The large displacement appearing in the region from 100 to 200 mm is a result of weak magnetic focusing and weak electric defocusing. Figure 7–8 shows the intensity distribution of the beam current as a function of the acceleration radius. In this case, the reeds of phase selector are fully opened. The beam intensity drops sharply at the radius of 200 mm, and in the outer region, the variation of the beam intensity is small. This fact accords with the displacement amplitude distribution in Fig. 7–6. Ions are lost most seriously by striking the edge of the dee or the dummy dee in the region from 100 to 200 mm radius. Also it is to be noticed that the sharp drop of beam current in Fig. 7–8 corresponds to the dip of beam current in Fig. 7–5 at 180 mm radius.

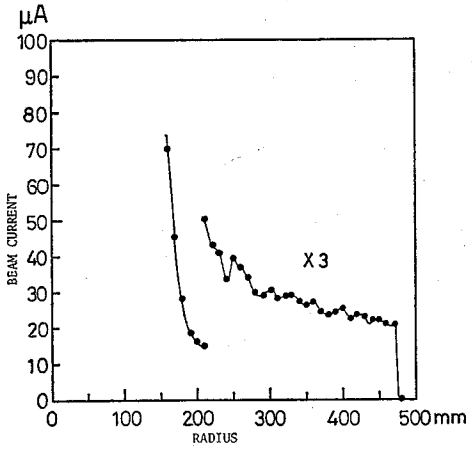

Fig. 7–8. Radial distribution of beam current.

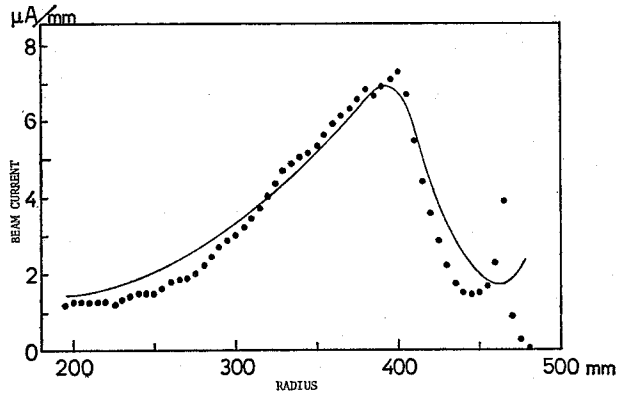

Fig. 7–9. Differential distribution of beam current. The solid line indicates the reciprocal of the turn separation of the beam.

To investigate the horizontal motion of the beam, the intensity distribution was measured by a current probe of differential type. This probe can detect the beam current with a resolution of 2 mm wide. Figure 7–9 shows the ion current density distribution as a function of the acceleration radius. The solid line in the figure indicates the reciprocal of the turn separation which is calculated on the basis of the assumptions that the dee voltage is 100 kV, the phases of the ions crossing the acceleration gap are given in Fig. 7–7 and the magnetic field distribution is given in Fig. 2–2. The solid line is normalized at 400 mm radius. The shape of the current density distribution agrees well with the prediction obtained from the turn separation calculation. This good agreement is a consequence of the fact that the beam is lost scarcely in the region of larger than 200 mm radius as shown in Fig. 7–8.

The optimum operating condition was searched and the results are shown in Figs. 7–10 and 7–11. The frequency of acceleration was fixed to 13.00 MHz and the magnetic field was varied to get maximum beam current. Figure 7–10 shows the distribution of the maximum beam current which was obtained by adjusting the magnetic field at each

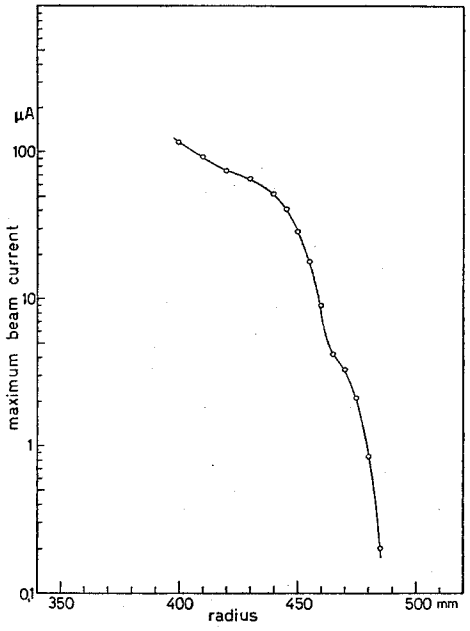

Fig. 7–10. Optimized radial distribution of beam current.

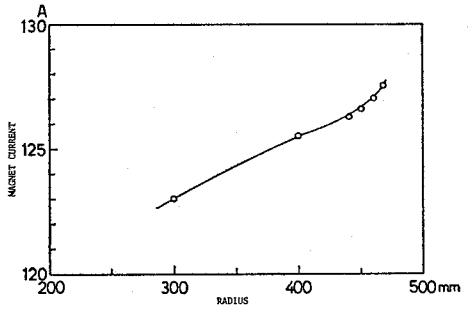

Fig. 7–11. Magnet current variation to get the maximum beam current.

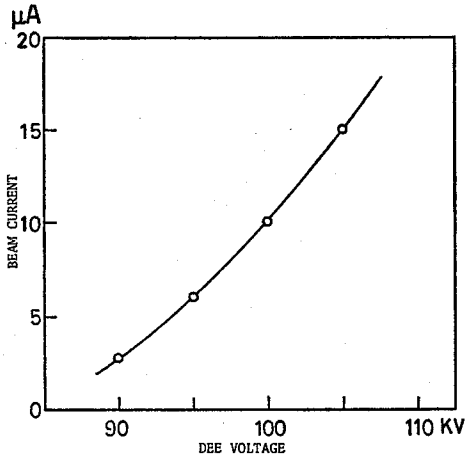

Fig. 7–12. Relation between the beam current and the dee voltage at maximum acceleration radius (=47 cm).

position of the beam probe. Figure 7–11 shows the magnet current variation to get the maximum beam current. The shape of beam current distribution is very much alike to that obtained in the case of the old cyclotron.[1)]

Figure 7–12 shows the beam current obtained at 47 cm radius when the dee voltage was varied. The oscillation frequency and the magnetic field were fixed. As seen in the figure, minimum dee voltage to accelerate ions to the final radius (=47 cm) is about 90 kV.

VII.3. Beam Extraction

The structure of the deflector is described in section V. The position and the direction of the deflector are adjustable in some limited range. In the first stage, the position of the septum was set at 47 cm radius and the position of the deflector exit was varied to get a beam of relevant direction. If the beam is extracted too outward, the beam strikes the pillar of the pole tip supporting device and if the beam goes too inward, the beam strikes the yoke of the main magnet. Available beam direction was planned on a figure and this direction was estimated by measuring the beam profile

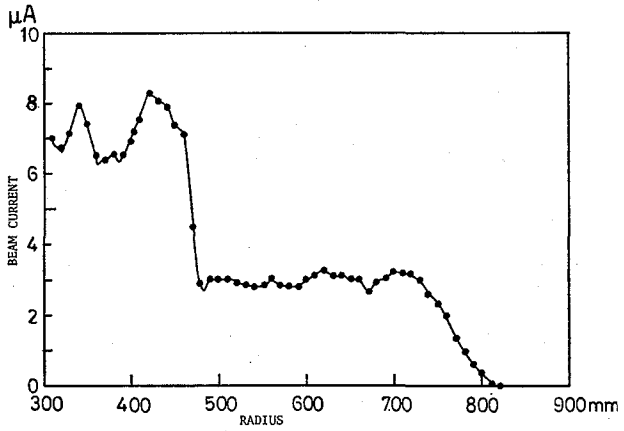

Fig. 7–13. Beam current obtained by the probe when the deflector voltage is applied.

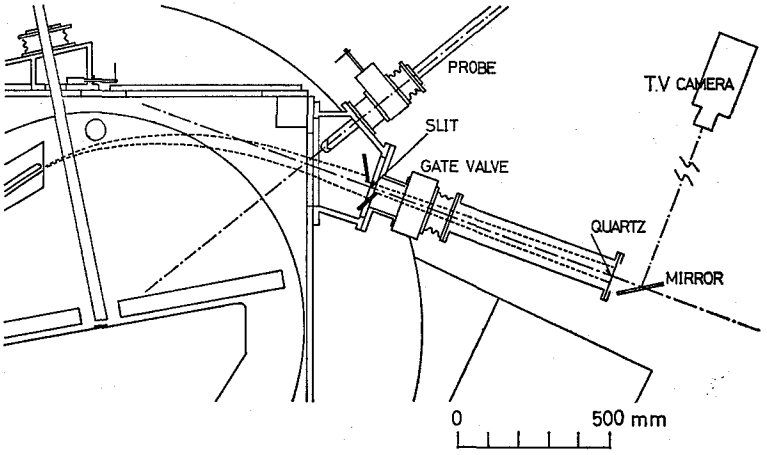

Fig. 7–14. Layout of the beam exit. Beam orbit is also shown.

at the position of beam current probe. Results obtained after several trials are shown in Fig. 7–13. In this case, the separation distance between septum and deflector electrode is 8 mm at its entrance and 10 mm at the exit. The exit was set at 53 cm radius from the center of the magnet. The applied voltage was 82 kV. The beam profile was estimated by using the beam probe. As seen in Fig. 7–13, the extraction efficiency is about 40% and the beam fans out in a range of about 60 mm at the position of the beam probe. The spread of the beam direction was measured further by setting a slit and a quartz plate 85 cm apart from the slit as shown in Fig. 7–14. The fan out angle of the beam profile was estimated to be 8°. This spread can be reduced by the use of a magnetic channel of which the description is given in section V.

VIII. SITE AND BUILDING

The cyclotron is installed in the building of the Nuclear Science Research Facility. Figure 8–1 shows the present arrangement of the Facility and this arrangement is the same as reported in Ref.[2] The layout of the cyclotron and beam lines is shown in Fig. 8–2. The motor driven doors at the east side and south side of the cyclotron area were constructed newly during the period of cyclotron improvement. A cooling tower of 7.8×10^5 kcal/hr capacity was also installed. The location of the cooling tower is outside of the building and is not shown in the figure.

The distribution station of electric power was renewed completely and lines of the power supply to the cyclotron component were also newly constructed. Radiation monitoring posts were prepared around the building of the Facility and the interlock system for the radiation safeguard was equipped at every entrance to the cyclotron area and experimental area. The works above mentioned were achieved simultaneously with the construction of the new cyclotron.

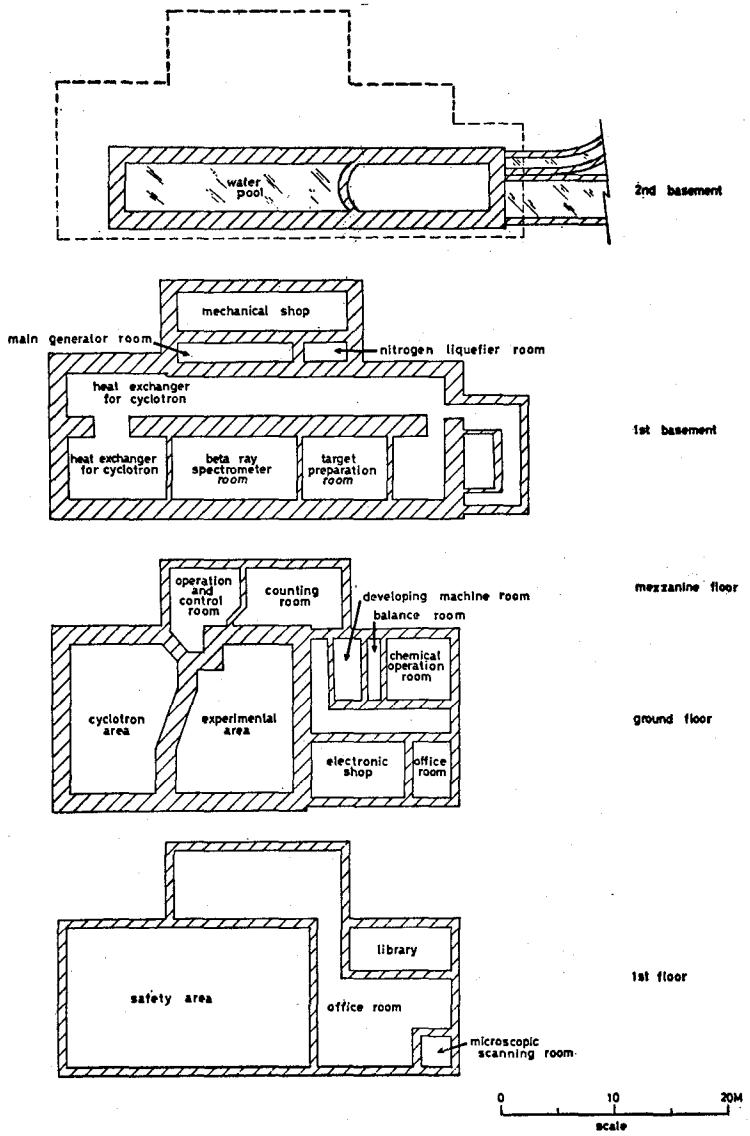

Fig. 8–1. Present arrangement of the Nuclear Science Research Facility.

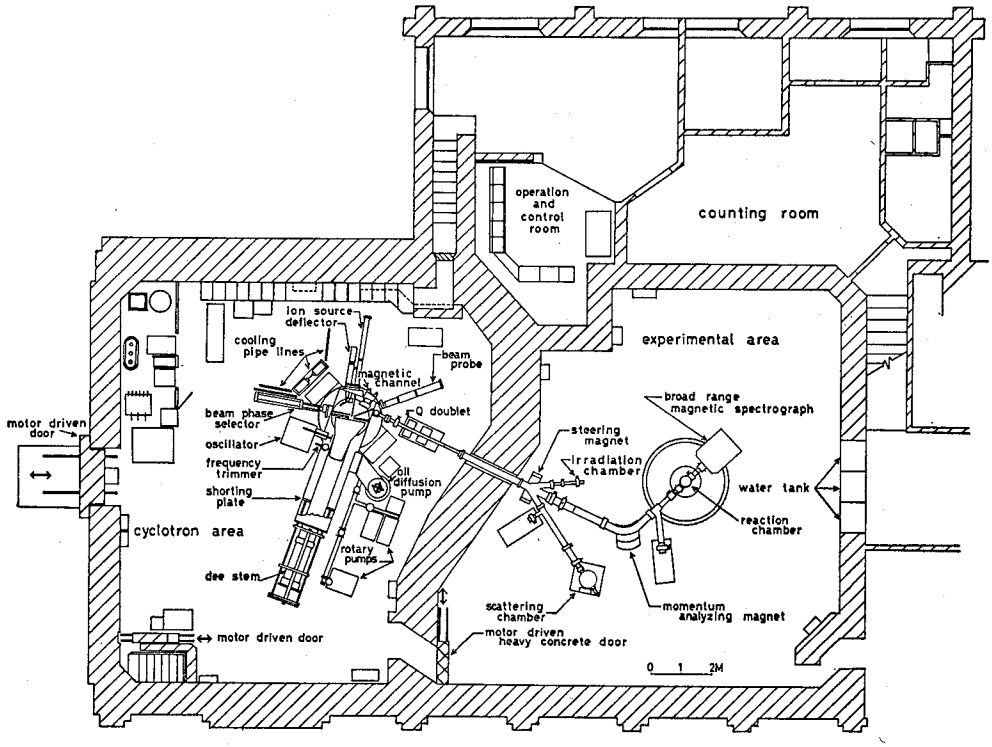

Fig. 8–2. Layout of the cyclotron and beam lines. The right hand side of the building faces to the north.

ACKNOWLEDMENTS

The improvement of the cyclotron was achieved by the help and good will of innumerable persons. Especially the authors would like to acknowledge the authorities of the Kyoto University and of the Ministry of Education for their financial support of this work. Also we would like to thank the past directors of the Institute for Chemical Research, Professor Dr. Waichiro Tsuji and Professor Dr. Sango Kunichika and the present Director of the Institute, Professor Dr. Eiji Suito for their arrangements and encouragements. The ion acceleration system was manufactured by the Mitsubishi Heavy Industries, the oscillator system by the Fuji Electronic Industrial Co., the evacuating system by the Shimazu Seisakusho, Ltd., the operation and control system by the Japan Panel Service Inc. and the deflector power source by the Origin Electric Co., Ltd. The patient co-operation and skilled working of the staffs of these companies are especially acknowledged; without the help of these persons, the improvement was to be sure impossible. Finally, we are very much obliged to Dr. S. Matsuki, Dr. K. Hosono and Dr. M. Yasue for their enlightening discussions given in the design stage of the improvement. Mr. S. Tanaka helped us to construct and operate the cyclotron. We like to thank him for his co-operation.

REFERENCES

(1) K. Kimura, Y. Uemura, M. Sonoda, S. Shimizu, T. Yanabu, R. Ishiwari, J. Kokame, A. Katase, I. Kumabe, S. Yamashita, H. Takekoshi, K. Miyake, H. Ikegami, and H. Fujita: *Bull. Inst. Chem. Res., Kyoto Univ.*, **39**, 368 (1961).

(2) K. Kimura: *Bull. Inst. Chem. Res.*, Kyoto Univ., **43**, 499 (1965).

(3) Y. Uemura and J. Kokame: *Shinku*, **4**, 20 (1961). Y. Uemura, A. Fujinaga, M. Gotoh, and M. Michishima: *Shitsuryo-bunseki*, **11**, 100 (1958).

(4) M. Odera, Y. Miyazawa, T. Tonuma, M. Hemmi, and O. Terajima: *Nucl. Inst. Meth.*, **65**, 247 (1968).